CENTRO DE INVESTIGACIONES EN ÓPTICA, A.C.

Optical classification of liquid solutions by means of a single Gaußlet; an application on the determination of glucose concentration in transparent and turbid media

Thesis submitted in partial fulfillment of the requirements for the Ph.D. degree in science (Optics)

M.Sc. Francisco Joel Cervantes Lozano

Advisor:

Dr. Moisés Cywiak Garbarcewicz

"Versión definitiva"

Diciembre de 2014
León, Guanajuato, México

DEDICATION

This dissertation is dedicated to my Family, who always supported me with their patience and understanding.

GRATEFULNESS

I thank to CONACYT for the economic support during my Ph.D. studies in Sciences (Optics). Likewise, I want to say thanks to the staff of Centro de Investigaciones en Óptica A.C. whom gave me all support during my stay in this research center.

Also, I special thanks to my advisor Doctor Moi (Moisés Cywiak Garbarcewics) for his patience and for all discussions (academic and non academic) that we have had to this day. No doubt, these discussions helped me to be a better professional but especially to be a better person. Also, I thank to my friends Octavius (Octavio Olvera Rábago), el Maestro (Juan Manuel Franco Sanchez), Buen Moi (Moisés Padilla Miranda) and Denia Navarro Villafaña for your friendship and for all the moments lost in discussions that did not lead anywhere.

Thanks to my mother, (Belem Lozano Olmos) for believe in me and for give me all her love. Thanks to my girlfriend Paola Pedroza for staying to my side in during this time. Thanks to Ulises Vega for his comprehension and for the support that he gave me during my studies.

Abstract

In this thesis we describe an optical technique that allows classifying liquid solutions by means of a single Gaublet[1]; specifically, the technique is based on measuring the semi-width of a single Gaussian focused probe beam while profiling a calibrated reflective grating by means of a specially devised homodyne detector which is described in the following section.

The probe beam consists of focusing a laser beam with a Gaussian intensity profile. To focus the beam a large working distance microscope objective is used as the focusing lens. The measurements are performed by placing the sample (solution under measurement) between the focusing lens and the detection plane. Changes in the refractive index of the sample result in variations in the size of the focused beam under measurement. An application of the technique for measuring glucose concentration in transparent and turbid media is presented. In the following sections we show how our proposal is applied for transparent samples as well as for turbid samples that simulate optical properties of biological tissues.

For clarity the presentation of the thesis is divided in chapters. In the first chapter we present an introduction with the backgrounds and the state of the art on the subject. In chapter two an analytic model of our proposal is presented. For convenience in chapter two we also present the description of the experimental setup that is used to measure the size of the focused beam. In chapter three we apply our technique for measuring glucose in thin transparent samples. In chapter four the technique is applied to samples containing a turbid medium which simulates optical properties of biological tissues. For convenience at the end of chapter four we discuss the accuracy of the technique and we give our error analysis. Finally, in chapter five we present our conclusions.

[1] A Gaußlet is a term which means Gaussian beamlet (a small beam of light) or “fat rays”, it was coined by Alan W. Greynolds (dx.doi.org/10.1364/IODC.2014.ITu1A.3).

Contents

Chapter 1

Introduction

From an optical point of view, the refractive index is one of the most important properties for characterizing an arbitrary material. This material, in general can be in solid, liquid or gaseous state. In particular, calculating the refractive index of a solution is of major importance. Even more, it is very significant to know the accurately dependence of the refractive index of a solution as a function of concentration. Due to this importance many techniques have been developed to accomplish this goal; for the best of our knowledge the techniques reported only described the methodology of the measurements and its correspond range of applicability and there is not an (optical) analytical model which may be used to predict physically the shape of the graph that exhibits the refractive index as a function of concentration of a solution. Furthermore, by reviewing the literature one can find discrepancies of the reported plots, specifically as in the case of our interest, if the solution concentration is composed of glucose [1-5]. The method that will we describe in the next sections can be applied to transparent samples and also to samples exhibiting turbid media. Our experiments were conducted with liquid solutions containing glucose and the samples were placed in thin containers

The importance of glucose is understandable as glucose is a carbohydrate nutrient source. Additionally it is important in industry as it is involved in many applications and in almost all biological processes. Due to this, glucose monitoring plays an important role. Glucose monitoring can be divided in two ranges, high and low concentrations. For instance, high concentrations techniques are necessary to monitoring the satisfactory production of 2,3-BDO using DNS and GRAS methods [6, 7] between others. By the other hand, if we talk about low concentrations (less than 10%) elaborate techniques have been developed to accomplish this aim; for example surface-plasmon resonance (SPR) [8-11] and fiber optics techniques [12, 13]. Also, it is important to remark that the referred techniques require large samples and are focused in describing the measurements and its

range of applicability. The techniques referred before are mainly designed to be applied in some area of biomedicine, as it is the case of detecting and monitoring a disease as it can be diabetes.

Glucose monitoring in biomedicine is based in obtaining blood of a living body and then process it as it can be by means of a plasma. In a living tissue it is also possible to measure its glucose concentration by means of some kind of tomography. In these two cases, the samples represent a turbid media or equivalently these samples represent scattering media. As it is apparent measurement of glucose concentration in thin turbid media with optical scattering properties representing real biological tissue is of major importance. These kinds of samples are usually performed by preparing models that represent biological tissue and are called phantoms. These phantoms are prepared in general using Intralipid ^{MR} or nanospheres [14-18]. In particular, Intralipid ^{MR} is a fat emulsion made with soy bean oil, egg phospholipids and glycerin and it is mainly used for patients who has problems to get nutrients from food through via an oral diet. Solutions of appropriate concentrations of Intralipid ^{MR} can be prepared to closely mimic the response of human or animal tissue to light at wavelengths in the red and infrared ranges where tissue is highly scattering but has a rather low absorption coefficient. Phantoms made of 1% Intralipid ^{MR} solution are commonly used for experiments that simulate optical scattering properties of biological tissues [19-21]. In chapter four this concepts are clarified.

Techniques to determine glucose concentrations in these samples can be classified mainly in two: by transmitted light and/or reflected light. When reflective light is used, the techniques are mainly of the type of optical coherence tomography (OCT), refractometric methods and Raman spectroscopy polarization [22-26]. These techniques generally exhibit low sensitivity (signal-to-noise-ratio), thus, requiring high glucose concentrations [24], resulting in imprecise values that require statistical algorithms to improve the estimation of the measurements. In contrast, techniques that use transmitted light are mainly based on the photo-acoustic effect (PA) [25, 27-32]. However, the PA signal can vary between measurements, meaning that differences of PA signal can be affected by other factors such as physiological change, temperature and mechanical stability of the sample [29].

In this research, we present a diffraction technique that permits calculate the general behavior of the refractive index of a solution as a function of concentration. We applied our technique when the concentration of the solution is based in glucose due to inherent importance as mentioned above; also, we apply our proposal to turbid samples that simulates optical properties of biological tissues.

Chapter 2

Analytical description

In this chapter we present our proposal, which is based in characterizing the main parameters of a Gaussian focused beam. We describe the theoretically basis to obtain the semi-width of the Gaussian probe beam at a plane of detection. In the next section we find an analytical relationship between the semi-width of the focused beam as a function of the refractive index of a sample, when this sample is placed between the lens and the plane of detection The experimental setup to perform the measurements is based in a homodyne knife-edge detector (KED) which is also described in this section. The propagation of the beam in its overall path from the laser beam up to the plane of detection, through the focusing lens and through the sample is performed by means of the Fresnel diffraction integral.

2.1 Gaussian beam propagation

We will begin our description with the experimental setup depicted in Fig. 1. A Gaussian beam emerges of a commercially available He-Ne laser which has a length wave of λ =632 nm. The beam is directed to a focusing lens which, in the absence of the sample, focuses the beam in a plane of observation denominated as x_6 in the figure. As mentioned, the system is adjusted properly to obtain the best focusing conditions at the referred plane of detection. For simplicity our description is a one-dimensional without any lose of generality. The liquid sample is poured in a thin container specially made that consists of parallel walls of thin glass. The sample containing the medium under study is placed between the focusing lens and the plane of detection. In order to assure parallelism of the walls container, a laser beam carefully aligned was aimed to the walls of the container and the reflected beams were monitored.

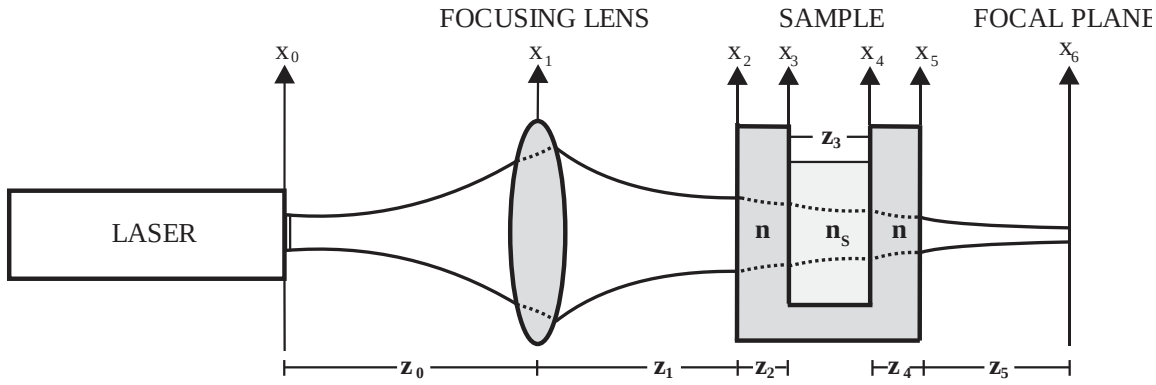

Fig. 1 Schematic representation of the Gaussian beam propagation through the system.

Fig. 1 will now be used to describe analytically the overall propagation as follows:

1. The beam is propagated form the output of the laser up to the back surface of the lens a distance z_0 as shown in Fig.1 In the drawing the propagation is performed from plane with coordinates x_0 up to the plane with coordinates x_1. We will assume that the lens is placed in the plane with coordinates x_1.

2. Next, we introduce the phase function introduced by the lens as the beam is transmitted through it.

3. Then the propagation from the output of the lens up to the left surface of the sample is calculated. This propagation is performed from the coordinate axes $x_1 \text{ to } x_2$, a distance z_1.

3. Now, the beam is propagated a distance z_2 inside the first wall of the container which exhibits a refractive index of value n. This propagation is performed between the planes $x_2 \text{ to } x_3$.

4. The beam travels a distance z_3 inside a solution with a refractive index n_S. The propagation is now performed from the right face of the first surface of the container up to the left surface of the second wall of the container. This propagation is performed between the planes $x_3 \text{ to } x_4$.

5. Next, the light propagates a distance z_4 inside the second wall of the container with a refractive index n. Thus, the propagation between planes $x_4 \text{ to } x_5$ is performed.

6. Finally, the beam propagates a distance z_5 from the right face of the second surface of the container up to the plane of detection. Thus, the propagation from planes x_5 to x_6 is performed.

The Gaussian beam distribution at the output of the laser at x_0 is represented as,

$$\Psi_0(x_0) = A_0 \exp\left(-\frac{x_0^2}{r_0^2}\right), \tag{1}$$

where A_0 is a constant amplitude that can be expressed in a closed form and as it will be apparent form the results its value results unimportant. The exponential term represents the Gaussian shape; r_0 is the beam semi-width and x_0 represents the coordinate of the plane at the output of the laser.

As mentioned, the Fresnel diffraction integral is used to calculate the field distribution at plane x_1 before reaching the lens. The corresponding equation is given as,

$$\Psi_1(x_1) = \frac{\exp\left(i\frac{2\pi z_0}{\lambda}\right)}{\sqrt{i\lambda z_0}} \int_{-\infty}^{\infty} A_0 \exp\left(-\frac{x_0^2}{r_0^2}\right) \exp\left[\frac{i\pi}{\lambda z_0}(x_0 - x_1)^2\right] dx_0 \ . \tag{2}$$

Expanding the term in the square brackets and simplifying we obtain

$$\Psi_1(x_1) = \frac{A_0}{\sqrt{i\lambda z}} \exp\left(i\frac{2\pi z_0}{\lambda}\right) \exp\left(i\frac{\pi}{\lambda z_0}x_1^2\right) \mathcal{F}\left\{\exp\left[-\pi\left(\sqrt{\frac{\lambda z_0 - i\pi r_0^2}{\pi r_0^2 \lambda z_0}}x_0\right)^2\right]\right\}_{u=\frac{x_1}{\lambda z_0}} . \tag{3}$$

It will be seen that the last term in Eq. (3) is the Fourier transform of a well known complex function. Thus, performing the Fourier transform [33] allows to write Eq. (3) as,

$$\Psi_1(x_1) = A_1 \exp\left(-\frac{x_1^2}{r_1^2}\right) \exp\left(i\beta_1 x_1^2\right), \tag{4}$$

where

$$A_1 = \frac{\exp\left(i\frac{2\pi z_0}{\lambda}\right)}{\sqrt{i\lambda z_0}} \sqrt{\frac{\pi r_0^2 \lambda z_0}{\lambda z_0 - i\pi r_0^2}} \tag{5a}$$

$$r_1 = \frac{\sqrt{\lambda^2 z_0^2 + \pi^2 r_0^4}}{\pi r_0} \tag{5b}$$

$$\beta_1 = \frac{\pi}{\lambda z_0}\left[1 - \frac{\pi^2 r_0^4}{\lambda^2 z_0^2 + \pi^2 r_0^4}\right]. \tag{5c}$$

Eq. (4) represents the field distribution of the Gaussian beam at the plane x_1, just before reaching the lens. We emphasize that the beam at this plane is again a Gaussian distribution where, A_1 represents its complex amplitude, r_1 is the semi-width and β_1 is a constant term which represents a divergent quadratic phase.

Now, the transmittance phase of the lens is introduced. For simplicity we will consider only quadratic phase factor and without loss of generality a more complex function can be introduce. The simplest way to do this is by updating the value of β_1 as: $\beta_1 - \pi/\lambda f$, being f the focal length of the lens. With Eq. (4) updated now we proceed in propagating the beam form the plane x_1 to the plane x_2. The amplitude distribution of the beam at his plane is denoted as $\Psi_2(x_2)$ and is given as,

$$\Psi_2(x_2) = \frac{\exp\left(i\frac{2\pi z_1}{\lambda}\right)}{\sqrt{i\lambda z_1}} \int_{-\infty}^{\infty} A_1 \exp\left(-\frac{x_1^2}{r_1^2}\right)\exp\left(i\beta_1 x_1^2\right)\exp\left[\frac{i\pi}{\lambda z_1}(x_1 - x_2)^2\right] dx_1 \tag{6}$$

solving Eq. (6) we obtain the following result,

$$\Psi_2(x_2) = A_2 \exp\left(-\frac{x_2^2}{r_2^2}\right)\exp\left(i\beta_2 x_2^2\right), \tag{7}$$

where

$$A_2 = A_1 \frac{\exp\left(i\frac{2\pi z_1}{\lambda}\right)}{\sqrt{i\lambda z_1}} \sqrt{\frac{\pi^2 r_1^2 \lambda z_1}{\lambda \pi z_1 + i\pi r_1^2(\beta_1 \lambda z_1 + \pi)}} \tag{8a}$$

$$r_2 = \frac{\sqrt{\lambda^2 z_1^2 + r_1^4(\beta_1 \lambda z_1 + \pi)^2}}{\pi r_1} \tag{8b}$$

$$\beta_2 = \frac{\pi}{\lambda\, z_1}\left[1 - \frac{\pi^2\, r_1^4\left(\beta_1\, \lambda\, z_1 + \pi\right)}{\lambda^2\, z_1^2 + r_1^4\left(\beta_1\, \lambda\, z_1 + \pi\right)^2}\right]. \tag{8c}$$

The next propagation is in the first wall of the glass container with refractive index n. The Fresnel diffraction integral takes the following form,

$$\Psi_3\left(x_3\right) = \frac{\exp\left(i\,\frac{2\,\pi\, z_2}{\lambda}\right)}{\sqrt{i\,\lambda\, z_2}} \int_{-\infty}^{\infty} A_2 \exp\left(-\frac{x_2^2}{r_2^2}\right) \exp\left(i\beta_2 x_2^2\right) \exp\left[\frac{i\,\pi}{\lambda\, z_2}\left(x_2 - x_3\right)^2\right] dx_2 \tag{9}$$

Eq. (9) has the solution,

$$\Psi_3\left(x_3\right) = A_3 \exp\left(-\frac{x_3^2}{r_3^2}\right) \exp\left(i\,\beta_3 x_3^2\right) \tag{10}$$

where

$$A_3 = A_2\, \frac{\exp\left[i\,\frac{2\pi\, z_2}{\left(\frac{\lambda}{n}\right)}\right]}{\sqrt{i\left(\frac{\lambda}{n}\right) z_2}} \sqrt{\frac{\pi^2\, r_2^2 \left(\frac{\lambda}{n}\right) z_2}{\pi\left(\frac{\lambda}{n}\right) z_2 + i\,\pi\, r_2^2\left[\beta_2\left(\frac{\lambda}{n}\right) z_2 + \pi\right]}} \tag{11a}$$

$$r_3 = \frac{\sqrt{\left(\frac{\lambda}{n}\right)^2 z_2^2 + r_2^4\left[\beta_2\left(\frac{\lambda}{n}\right) z_2 + \pi\right]^2}}{\pi\, r_2} \tag{11b}$$

$$\beta_3 = \frac{\pi}{\left(\frac{\lambda}{n}\right) z_2}\left[1 - \frac{\pi^2\, r_2^4\left[\beta_2\left(\frac{\lambda}{n}\right) z_2 + \pi\right]}{\left(\frac{\lambda}{n}\right)^2 z_2^2 + r_2^4\left[\beta_2\left(\frac{\lambda}{n}\right) z_2 + \pi\right]^2}\right]. \tag{11c}$$

Now, we need to propagate the beam in a solution with refractive index n_S. The field distribution is represented by,

$$\Psi_4(x_4) = \frac{\exp\left(i\frac{2\pi z_3}{\lambda}\right)}{\sqrt{i\lambda z_3}} \int_{-\infty}^{\infty} A_3 \exp\left(-\frac{x_3^2}{r_3^2}\right) \exp\left(i\beta_3 x_3^2\right) \exp\left[\frac{i\pi}{\lambda z_3}(x_3 - x_4)^2\right] dx_3 \qquad (12)$$

the solution of Eq. (12) is the next

$$\Psi_4(x_4) = A_4 \exp\left(-\frac{x_4^2}{r_4^2}\right) \exp\left(i\beta_4 x_4^2\right) \qquad (13)$$

where the constants take the next values,

$$A_4 = A_3 \frac{\exp\left[i\frac{2\pi z_3}{\left(\frac{\lambda}{n_S}\right)}\right]}{\sqrt{i\left(\frac{\lambda}{n_S}\right)z_3}} \sqrt{\frac{\pi^2 r_3^2 \left(\frac{\lambda}{n_S}\right) z_3}{\pi\left(\frac{\lambda}{n_S}\right) z_3 + i\pi r_3^2 \left[\beta_3\left(\frac{\lambda}{n_S}\right) z_3 + \pi\right]}} \qquad (14a)$$

$$r_4 = \frac{\sqrt{\left(\frac{\lambda}{n_S}\right)^2 z_3^2 + r_3^4 \left[\beta_3\left(\frac{\lambda}{n_S}\right) z_3 + \pi\right]^2}}{\pi r_3} \qquad (14b)$$

$$\beta_4 = \frac{\pi}{\left(\frac{\lambda}{n_S}\right) z_3} \left[1 - \frac{\pi^2 r_3^4 \left[\beta_3\left(\frac{\lambda}{n_S}\right) z_3 + \pi\right]}{\left(\frac{\lambda}{n_S}\right)^2 z_3^2 + r_3^4 \left[\beta_3\left(\frac{\lambda}{n_S}\right) z_3 + \pi\right]^2}\right]. \qquad (14c)$$

after that, the next propagation is in the second wall of the glass container taking the refractive index as n. The field distribution takes the next form,

$$\Psi_5(x_5) = \frac{\exp\left(i\frac{2\pi z_4}{\lambda}\right)}{\sqrt{i\lambda z_4}} \int_{-\infty}^{\infty} A_4 \exp\left(-\frac{x_4^2}{r_4^2}\right) \exp\left(i\beta_4 x_4^2\right) \exp\left[\frac{i\pi}{\lambda z_4}(x_4 - x_5)^2\right] dx_4 \quad (15)$$

Eq. (15) has the following solution,

$$\Psi_5(x_5) = A_5 \exp\left(-\frac{x_5^2}{r_5^2}\right) \exp\left(i\beta_5 x_5^2\right) \quad (16)$$

where

$$A_5 = A_4 \frac{\exp\left[i\frac{2\pi z_4}{\left(\frac{\lambda}{n}\right)}\right]}{\sqrt{i\left(\frac{\lambda}{n}\right)z_4}} \sqrt{\frac{\pi^2 r_4^2 \left(\frac{\lambda}{n}\right) z_4}{\pi\left(\frac{\lambda}{n}\right)z_4 + i\pi r_4^2\left[\beta_4\left(\frac{\lambda}{n}\right)z_4 + \pi\right]}} \quad (17a)$$

$$r_5 = \frac{\sqrt{\left(\frac{\lambda}{n}\right)^2 z_4^2 + r_4^4\left[\beta_4\left(\frac{\lambda}{n}\right)z_4 + \pi\right]^2}}{\pi r_4} \quad (17b)$$

$$\beta_5 = \frac{\pi}{\left(\frac{\lambda}{n}\right)z_4}\left[1 - \frac{\pi^2 r_4^4\left[\beta_4\left(\frac{\lambda}{n}\right)z_4 + \pi\right]}{\left(\frac{\lambda}{n}\right)^2 z_4^2 + r_4^4\left[\beta_4\left(\frac{\lambda}{n}\right)z_4 + \pi\right]^2}\right]. \quad (17c)$$

Finally, we calculate the propagation from the right face of the second wall of the container to the plane of observation, axis x_6. At this plane the field distribution is given as,

$$\Psi_6(x_6) = \frac{\exp\left(i\frac{2\pi z_5}{\lambda}\right)}{\sqrt{i\lambda z_5}} \int_{-\infty}^{\infty} A_5 \exp\left(-\frac{x_5^2}{r_5^2}\right) \exp\left(i\beta_5 x_5^2\right) \exp\left[\frac{i\pi}{\lambda z_5}(x_5 - x_6)^2\right] dx_5 . \quad (18)$$

Performing the integral in Eq. (18) in a similar way as in the above calculations, we obtain,

$$\Psi_6(x_6) = A_6 \exp\left(-\frac{x_6^2}{r_6^2}\right)\exp\left(i\,\beta_6 x_6^2\right) \tag{19}$$

where

$$A_6 = A_5 \frac{\exp\left(i\frac{2\pi z_5}{\lambda}\right)}{\sqrt{i\lambda z_5}}\sqrt{\frac{\pi^2 r_5^2 \lambda z_5}{\lambda\pi z_5 + i\pi r_5^2(\beta_5 \lambda z_5 + \pi)}} \tag{20a}$$

$$r_6 = \frac{\sqrt{\lambda^2 z_5^2 + r_5^4(\beta_5 \lambda z_5 + \pi)^2}}{\pi r_5} \tag{20b}$$

$$\beta_6 = \frac{\pi}{\lambda z_5}\left[1 - \frac{\pi^2 r_5^4(\beta_5 \lambda z_5 + \pi)}{\lambda^2 z_5^2 + r_5^4(\beta_5 \lambda z_5 + \pi)^2}\right]. \tag{20c}$$

Eq. (19) describes the field distribution at the plane of observation. The semi-width of the laser beam, which is the main parameter of our proposal is given in Eq. (20b).

To proceed further we choose different values of n_S and with the aid of Eq. (20b) we tabulate them against r_6. Table 1(below) shows the values obtained.

$r_6\,(\mu m)$	n_S	$r_6\,(\mu m)$	n_S
1	1.33128	1.336	1.33788
1.003	1.33188	1.391	1.33848
1.012	1.33248	1.448	1.33908
1.027	1.33308	1.507	1.33968
1.049	1.33368	1.569	1.34028
1.076	1.33428	1.632	1.34088
1.109	1.33488	1.696	1.34148
1.147	1.33548	1.762	1.34208
1.189	1.33608	1.828	1.34268
1.234	1.33668	1.896	1.34328
1.283	1.33728	-	-

Table 1. Values of r_6 obtained with Eq. (20b) for different values of n_S.

The values tabulated in Table 1 are plotted in Fig. 2 (dotted plot). Additionally a curve fitted by a least square method is also shown in the figure (the solid plot). The fitted equation is given as,

$$n_S = 1.3313 + 41.84\left(r_6 - 1\times10^{-6}\right)^{0.5881} \tag{21}$$

where n_S is the refractive index of the solution and r_6 is the semi-width in the axis x_6.

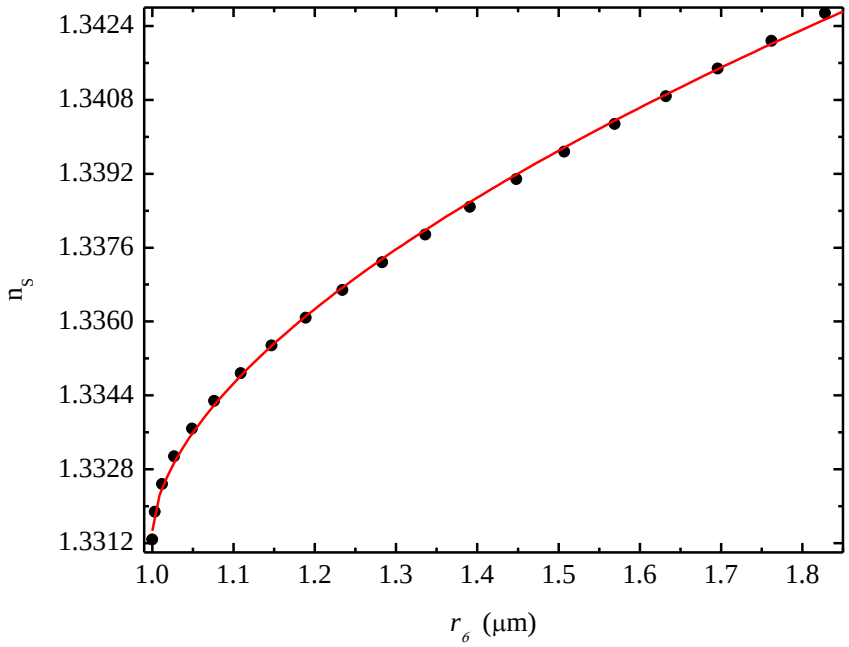

Fig. 2. Theoretical dependence of the refractive index of the solution as a function of the semi-width r_6. Dots correspond to calculations obtained by diffraction. The solid line is the fitted curve

Fig. 2 reveals an important physical effect. When the system is adjusted to optimal focusing conditions (r_6 =1 μm and n_S =1.3312), we can observe that large variations of the refractive index n_S result in small changes of the semi-width r_6. We can explain this as follows, when the Gaussian beam remains approximately collimated over the beam waist region it is found in the Rayleigh range. Further increments of the refractive index cause large variations of the semi-width now outside the Rayleigh range. It is important to remark that the plot in Fig. 2 be located in the Rayleigh region and extends into a small region outside it.

Now, it is necessary to find how the refractive index is related to the concentration of the solution, which hereafter will be denoted as c. In this way, we need to find how c depends on r_6. We will limit our discussion to substances where n_S increases with c, in the following manner.

Initially, when the concentration is low it is reasonable to expect linearity between c and r_6. Increments of c will only cause small increments of r_6 as we reside into the Rayleigh region. Subsequent increases of c, now outside of the Rayleigh region, will cause larger increments of r_6 (now not necessarily linear) until the solution approach the saturation which will cause r_6 to approach asymptotically to a certain finite value. This physical behavior can be represented by three regions which we denote accordingly as the Rayleigh region, the free region and the saturation region or equivalently regions I, II and III. For each region it is possible to propose qualitatively a relation of r_6 as a function of c. This relation must be substitute in Eq. (21). In Fig. 3 we show qualitatively the shape of the expected plot for a hypothetical solution which includes the three regions.

To demonstrate experimentally our previous theory we performed measurements with glucose solutions at low concentrations (less than 10 g/dl or equivalently less than 10 %) falling is a small vicinity between regions I and II. Additionally, as we are in a region of low concentration we expect a linear dependence of r_6 against c of the form

$$r_6(c) = K_1 + K_2\, c, \tag{22}$$

where the positive constants values K_m, $m = 1,2$ must be determined experimentally for each particular substance.

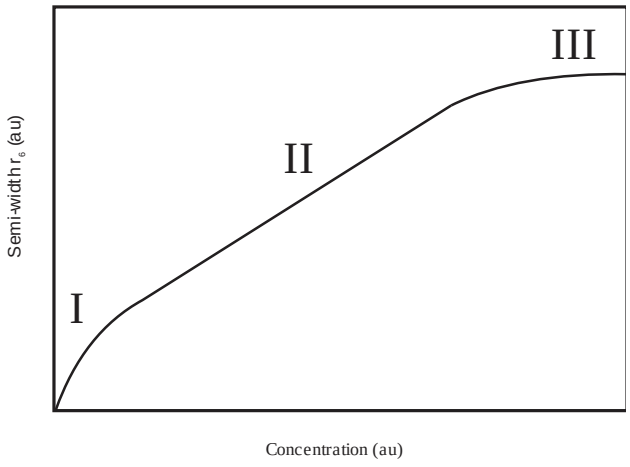

Fig. 3. Theoretical dependence of the semi-width r_6 as a function of the concentration. The plot consists of three regions as described in the text.

In our experiments the semi-width has to be measured with high accuracy; thus, we will used the homodyne Knife-Edge detector (KED) which results appropriate for our proposes. In the next section we will describe the KED.

2.2 Homodyne knife-edge detector to measure the semi width.

To measure the semi-width of the Gaussian probe beam, we take advantage that offers of the homodyne knife-edge detector (KED) [34-35]. The KED in its origins was designed to measure with high accuracy the profile of a surface. Additionally, the detector allows obtaining the roughness of the profile under test.

The setup of the KED is depicted in Fig. 4. A polarized He-Ne laser beam ($\lambda = 632\,\text{nm}$) is focused on the surface under test (SUT) which in our case is a calibrated holographic reflective grating. The focusing lens (L) is a 100 X microscope objective with a working distance of 1 cm allowing the properly placement of the sample. The probe beam, reflected by the grating, is sent for detection by means of a beam splitter (BS) to a half-blocked photodiode. As depicted in Fig. 4 the sample is placed between the focusing lens and the SUT, according to Fig. 4. An attenuator (A) is included to avoid damaging the grating due to excessive heating. A flexure mode piezoelectric transducer (PZT) vibrates the grating at approximately 10 Hz with small amplitude δ_0 in the x-direction as depicted and it is also used to mechanically scan the grating at a slow rate in the same direction. A lock-in amplifier is used to generate the vibration and to detect the AC signal from the photodiode. A personal computer (PC) adds the scanning signal and communicates with the lock-in by GPIB to automate the measurements

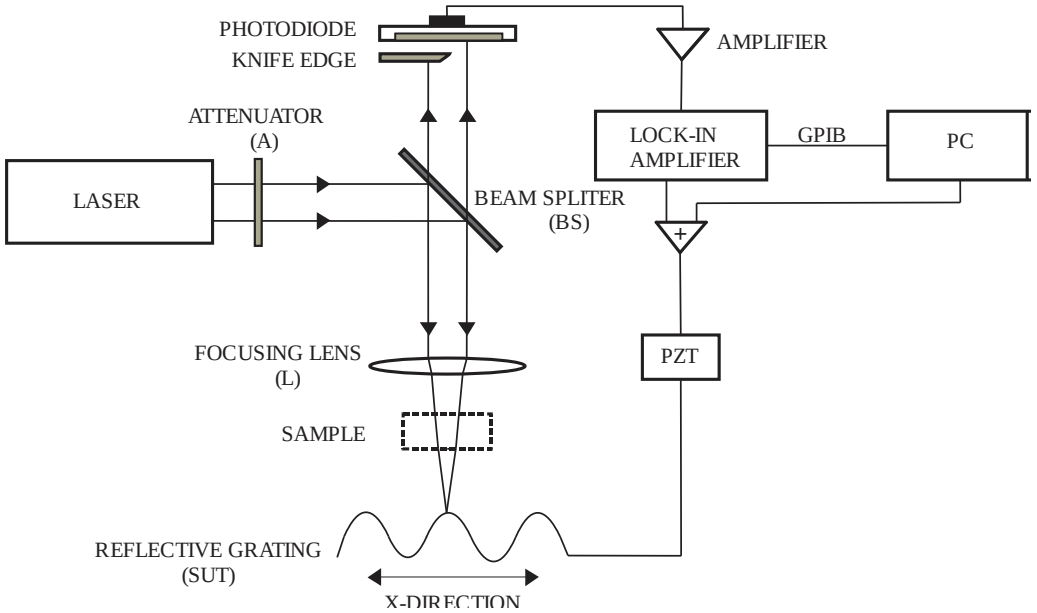

Fig. 4 Experimental setup of the KED.

The sample was introduced in a glass container which was constructed by our self to ensure that the walls be parallel and this way we avoid deflections of the beam that can affect the measurements. The dimensions of the container were 5.0 x 5.0 x 1.2 mm^3, where the light path is along the 1.2 mm width.

The AC power collected by the half-blocked photodiode is given by [34, 35]

$$P_{out}(x_6, y_6) = -i\frac{8P_0}{\lambda r_6^2}\delta_0 \int_{-\infty}^{\infty}\int_{-\infty}^{\infty} \exp\left(-2\frac{(x-x_6)^2+(y-y_6)^2}{r_6^2}\right) \mathrm{erf}\left(i\frac{x-x_6}{r_6}\right)\frac{\partial}{\partial x}h(x,y)\,dx\,dy, \tag{23}$$

where $i=\sqrt{-1}.$ and P_0 is the beam constant power. δ_0 is a small amplitude vibration of the piezoelectric transducer as described in [34, 35]. r_6 is the semi-width of the Gaussian beam and it is focused at (x_6, y_6)accordingly with coordinates of the back focal plane of the section 2.1. λ is the wavelength of the laser beam. erf() is the error function. $h(x_6, y_6)$ represents the profile of the SUT considered in a plane (x_6, y_6) to coincide with coordinates

in Fig. 1. The partial derivative of the height distribution appears as a consequence of a first order expansion due to the vibration of the SUT.

The integral in Eq. (23) represents the convolution of two functions. The first function is the derivate of the vertical height distribution of the surface under test. The second function is the impulse response of the system described as,

$$\Re(x_6, y_6) = -i\frac{8P_0\delta_0}{\lambda r_6^2}\exp\left(-2\frac{x_6^2+y_6^2}{r_6^2}\right)\mathrm{erf}\left(i\frac{x_6}{r_6}\right). \tag{24}$$

The profile is a sinusoidal reflective calibrated grating that can be represented as,

$$h(x,y) = h_0\left[1+\sin\left(\frac{2\pi}{\Lambda}x\right)\right], \tag{25}$$

where h_0 is the height amplitude of the grating and Λ is the period in the x-direction. Now, with this information Eq. (23) can be used to describe the behavior of the output power as a function of the defocus. After performing the integral given in Eq. (23), we obtain the detected power as,

$$P_{out}(x_6, y_6) = \frac{8\pi^2\delta_0}{\lambda\Lambda}P_0\exp\left(-\frac{\pi^2 r_6^2}{2\Lambda^2}\right)\mathrm{erf}\left(\frac{\pi r_6}{\sqrt{2}\Lambda}\right)\left[h_0\sin\left(\frac{2\pi}{\Lambda}x_6\right)\right]. \tag{26}$$

Eq. (26) shows that the power collected by the photodiode is proportional to the local vertical high of the grating and is a function of the horizontal spatial coordinate (x_6). It is independent of y_6 and is proportional to the local vertical height of the grating under test. The power depends also of the semi-width r_6 and the period of the grating Λ. The profiles are obtained by scanning a small region of the grating.

As we mentioned in the text, the system is adjusted to the best focusing conditions for zero glucose concentration ($r_6 = 1\mu m$). Then, when glucose concentration increases the semi-width also will increase and this in turn will cause a decrease of the vertical amplitude

recorded according with Eq. (25). Let us now consider two particular cases of reducing the vertical profiles to 75 and 50% with respect to the case c =0. The 600 lines/mm grating will require defocusing values of 1.08 and 1.19 μm respectively; these values correspond to samples with concentrations of 0.3 and 0.9 g/dl respectively. In contrast the grating of 300 lines/mm will require higher defocusing, 1.47 and 1.81 μm, corresponding to higher concentrations 4.5 and 7.5 g/dl [36]. Table 2 summarizes these results.

Decreasing amplitude (%)	Glucose concentration (g/dl) Λ_{600} / Λ_{300}	Semi-width (μm) Λ_{600} / Λ_{300}
75	0.3 / 4.5	1.08 / 1.47
50	0.9 / 7.5	1.19 / 1.81

Table 2. Experimental glucose concentrations and defocusing required for diminishing in 75 and 50 % of the maximum amplitude for both gratings: 600 and 300 lines/mm, for a thin transparent sample as reported in [36].

Fig. 5 shows a plot of the vertical amplitude normalized given by Eq. (26). These results demonstrate that the sensitivity of the system can properly be adjusted by only selecting the grating pitch.

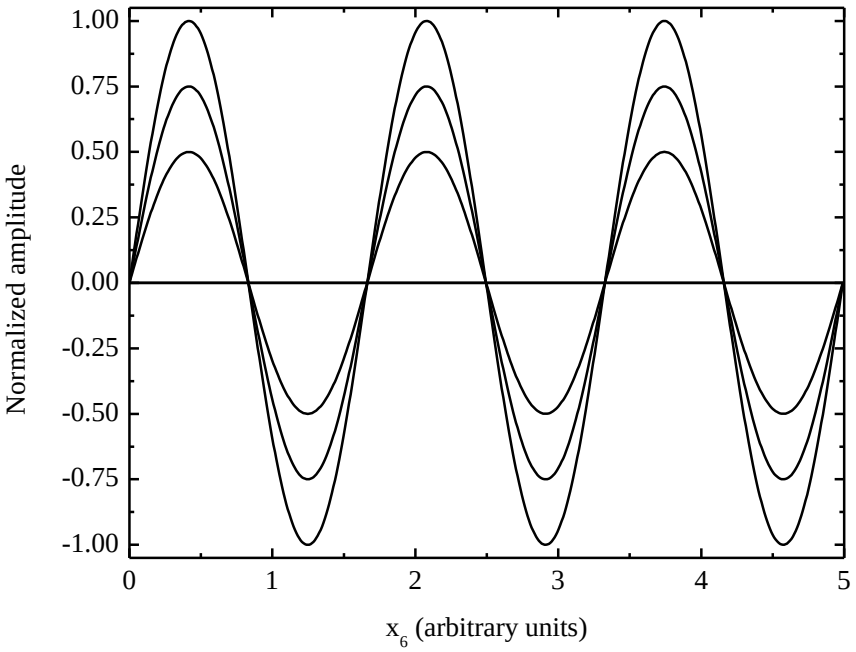

Fig. 5 Decrease of the vertical amplitudes as a function of defocus as described in the text.

In next section will describe the behavior of the decreasing of the vertical amplitude according to Eq. (26)

2.3 System response

In this section we will described the response of the system when it is adjusted to the best focusing conditions. Eq. (26) demonstrates that the power collected by the photodiode is proportional to the local vertical height of the grating, the term in square brackets. Thus, in order to record the vertical profile over a determined region, it is necessary to perform a linear scan. A plot of Eq. (26) for the two different gratings used in our experiments, 600 and 300 lines/mm is depicted in Fig. 6 for a constant local vertical height.

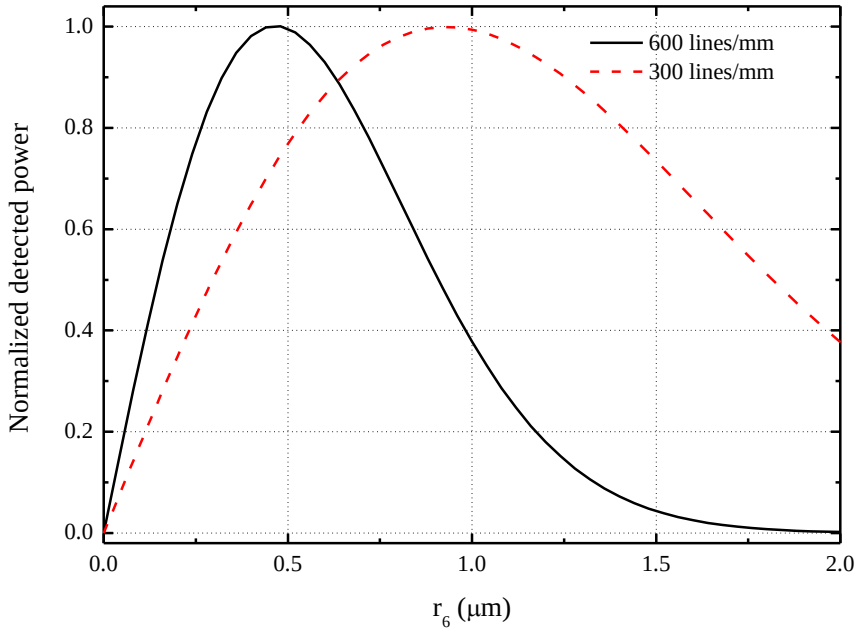

Fig.6 Normalized detected power as a function of r_6 according to Eq. (26) for gratings 600 and 300 lines/mm.

In our experiments, the best focusing conditions are obtained for $r_6 = 1$ μm. When glucose concentration increases the semi-width also increases, in this way we obtain bigger

values of r_6. It can be noticed from Fig. 6 that for both gratings the amplitude of the detected power decreases for $r_6 > 1$ μm. Fig. 6 also reveals that the sensitivity of the system can be tuned according to experimental requirements. The plot for the 300 lines/mm grating exhibits a less pronounced slope, being less sensitive than the curve for the 600 lines/mm plot which is more sensitive. Accordingly, increasing the pitch of the reflective grating will increase the sensitivity of the system and decreasing the pitch will decrease the sensitivity as required.

In the next chapter we give our experimental results.

Chapter 3

Experimental results for transparent samples

In this chapter, we describe the experimental results for the case of transparent samples. We describe the procedure for the preparation of the samples. We describe the experimental processes for the measurements using reflective gratings of 600 and 300 lines/mm. At the end of this chapter, we give experimental plots of the refractive index as a function of glucose concentration.

3.1 Sample preparation

To prepare our samples we used tri-distilled water for the zero concentration reference. For brevity henceforth this sample will be referred as the zero glucose concentration sample or 0 mg/dl. The system will be tuned to two different sensitivities. To achieve this, we will use two calibrated reflective gratings: 300 and 600 lines/mm. The grating with a pitch of 600lines/mm will be applied for measuring samples for glucose concentration from 0 to 1.25 g/dl. The second grating will be used with samples with concentrations in the range from 0 to 7.5 g/dl. The samples are prepared with a glucose patron of Dextrose Anhydrous commercially available.

The solutions were prepared as follows,

(a) For concentrations between 0 and 1.25 g/dl we took a recipient in which we poured 100 ml of tri-distilled water, this was a base sample. Then in other recipient we poured again 100 ml of tri-distilled water but this time we add noun amounts of glucose to obtain the glucose concentration desired. We prepared six samples in steps of 0.25 g/dl for 600 lines/mm grating.

(b) For concentrations between 0 and 7.5 g/dl we repeated the same procedure mentioned in point (a) but this time the steps of glucose were of 1.5 g/dl for the 300 lines/mm.

Table 3 summarize the sample preparations,

Samples of glucose concentration for Λ_{600} (g/dl)	Samples of glucose concentration for Λ_{300} (g/dl)
0	0
0.25	1.5
0.50	3.0
0.75	4.5
1.00	6.0
1.25	7.5

Table 3 Experimental samples prepared for both gratings 600 and 300 lines/mm.

3.2 Experimental procedure

For each grating the experimental procedure was as follows,

- First, the system was adjusted to the best focusing conditions with the sample of zero glucose concentration.
- Second, a region of the grating was scanned and recorded.
- After that, a know amount of glucose concentration was poured into the container and was left to settle.
- Then, the same region of the grating was scanned and recorded.

- Finally, we repeated the same process for each new glucose concentration.

We verify the repeatability of the measurements by scanning several times the same region. In each scan 200 pixels were recorded. All measurements were made a temperature constant of 25º C. Each measurement took approximately one minute. Additionally, it is important to remark that we were careful to assure that the transmittance of the sample remained constant.

3.3 Experimental results for 600 lines/mm grating

For measurements between 0 and 1.25 g/dl we used the 600 lines/mm grating. As we mentioned in the text above, this grating permits tune the sensitive of the system for low concentrations. Fig. 7 shows plots of the normalized vertical amplitudes for the concentrations before mentioned where small amplitudes corresponds to higher concentrations.

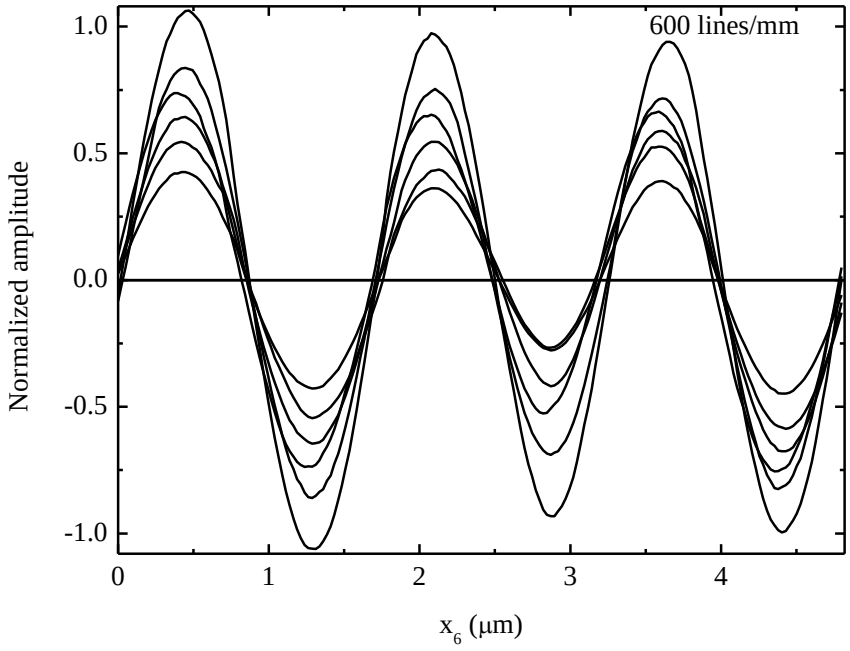

Fig.7 Experimental normalized vertical amplitude for 600 lines/mm grating. In the figure small amplitudes correspond to higher concentrations.

To improve the precision of the measurements we calculated the rms values of each vertical profile. Fig. 8 shows the rms values as a function of glucose concentration; each rms corresponds to the measurements depicted in Fig. 7.

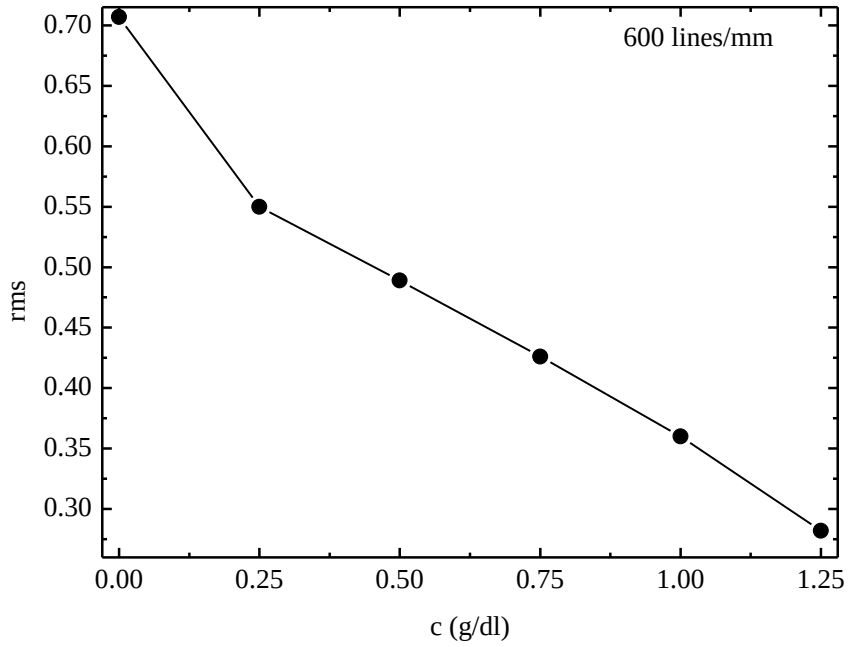

Fig. 8 Plot of the rms values of the normalized vertical heights of the normalized vertical profiles for 600 lines/mm grating as a function of glucose concentration.

We the above results we estimated that the minimum step of glucose concentration that we can detect for the 600 lines/mm grating is about of 0.06 g/dl.

3.4 Experimental result for the 300 lines/mm grating

The 300 lines/mm grating was used in the range between 0 and 7.5 g/dl. Fig. 9 depicts the normalized vertical profiles for these measurements. The smaller amplitudes correspond to higher concentrations.

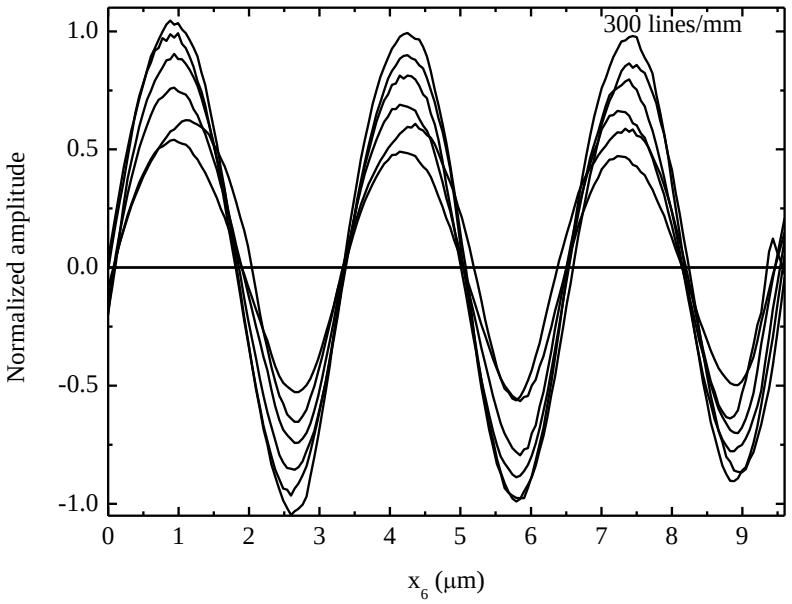

Fig.9 Experimental normalized vertical amplitude for 300 lines/mm grating. In the figure small amplitudes correspond to higher concentrations.

Fig 10 shows the rms values of the vertical profiles obtained in Fig. 9. With these results we estimated that the minimum step for measure glucose concentration is about 0.25 g/dl.

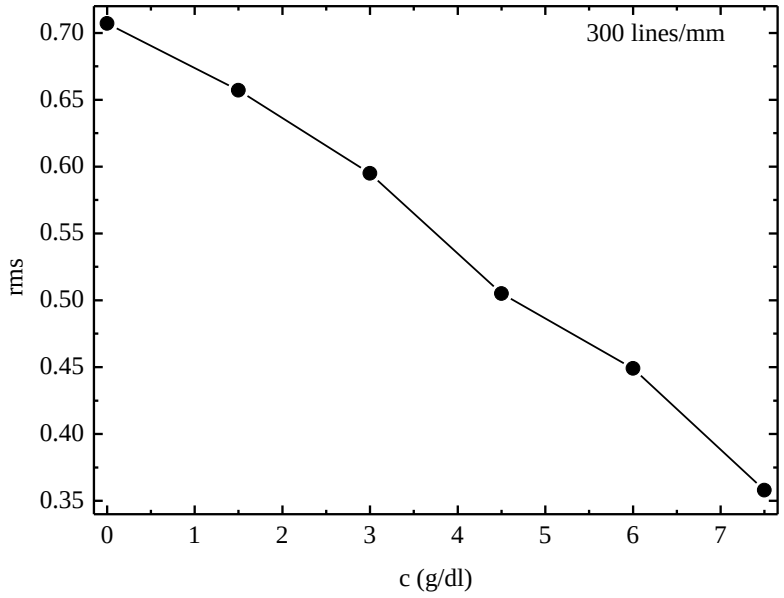

Fig.10 Plot of the rms values of the normalized vertical heights of the normalized vertical profiles for 300 lines/mm grating as a function of glucose concentration.

As we can see, the behavior of the vertical profiles measured in both cases is in agreement with Eq. (25). It is important to remark that we can use a laser with a shorter wavelength; this will permit us to use gratings with high spatial frequencies given the possibility of measure lower values of concentration.

3.5 General behavior of n_s as a function of c

With the results obtained in section 3.3 and 3.4 we can construct a overall plot of n_s as a function of c. To do this, first, we must to relate the semi-width (r_6) with changes in the concentration (c) of the sample: this relationship has to be in agreement with Eq. (22). To construct this relation we need to take the results of both gratings and put together in a plot. This can be done because the 600 lines/mm grating has a defocusing between 1 and 1.19 μm and the other one has a defocusing between 1 and 1.81 μm. This plot is shown in Fig. 11. As we mentioned in section 2.1 this behavior resides between regions I and II.

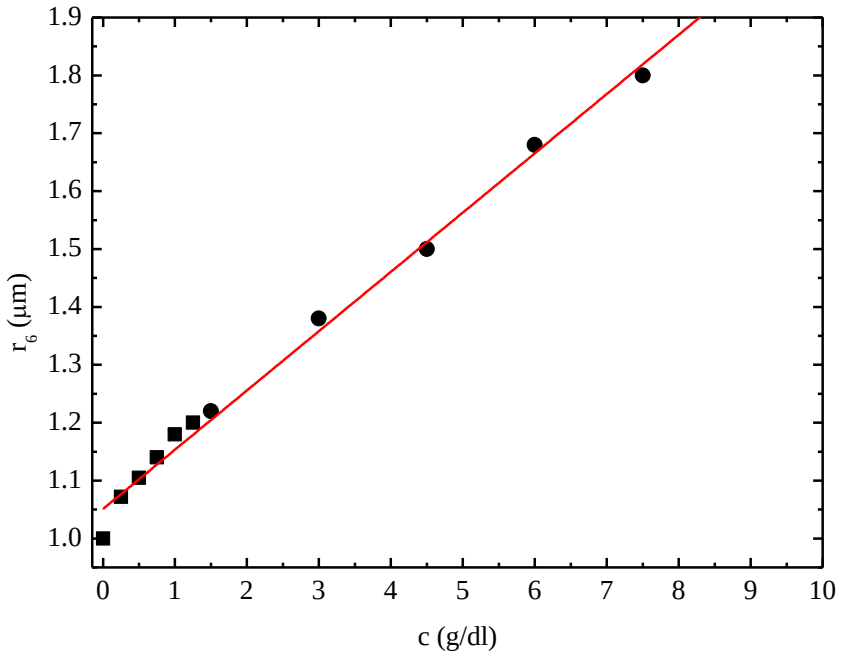

Fig.11 Plot of the experimentally semi-width r_6 as a function of glucose concentration c. The regions with squares symbols were obtained with the 600 lines/mm grating and the regions with circles was obtained with the 300 lines/mm grating.

In Fig. 11 the first part of the region was obtained with the 600 lines/mm grating and the corresponding symbols are squares; the second part of the region was obtained with the 300 lines/mm grating and their corresponding symbols are circles. Also it includes its corresponding fitted curve.

The fitted equation obtained is given by,

$$r_6(c) = 1.51\times10^{-6} + 1.024\times10^{-7}c \tag{27}$$

where c stands for glucose concentration measured in g/dl and r_6 is measured in microns. Eq. (27) is in agreement with the one predicted theoretically in Eq. (22). Now with this information we can relate n_S as a function of c. This can be done substituting Eq. (27) in Eq. (21) obtaining

$$n_S(c) = 1.3312 + 41.841\left(0.051\times10^{-6} + 1.024\times10^{-7}c\right)^{0.5881} \tag{28}$$

where, as indicated, c is the glucose concentration and n_S is the refractive index of the sample. Eq. (28) shows that for small values of concentration a linear relation is obtained as a function of the refractive index as we predicted in our theoretical description. A plot of Eq. (28) is shown in Fig. 12.

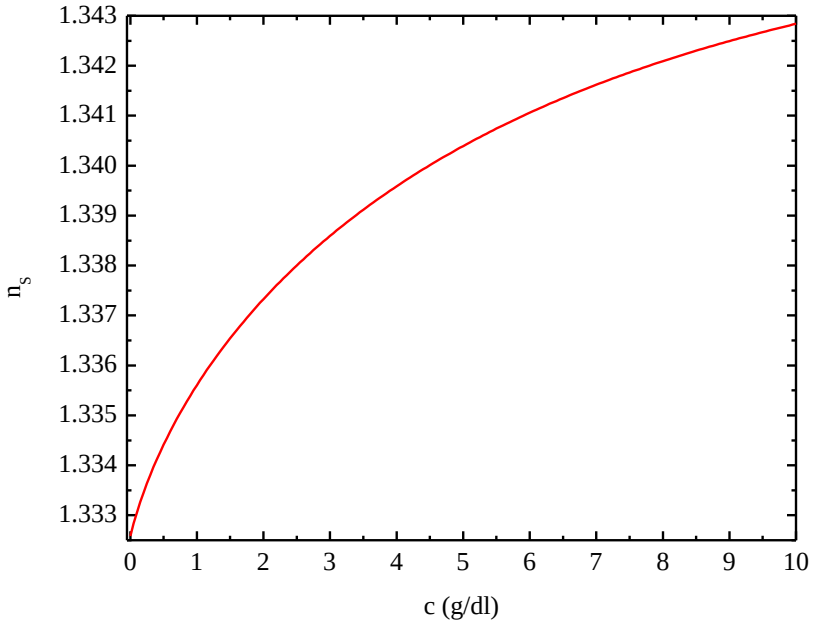

Fig.12 n_S as a function of c for $\lambda = 632\,\text{nm}$.

The plot in Fig. 12 shows the overall behavior of n_S as a function of c. The plot resides in region I and extends slightly into region II. It is important to notice how pitches of the grating were tuned to construct each particular region of the overall plot.

3. Comparison of our results compared with other techniques

For comparative purposes, we show in Fig. 13 a comparison between the results obtained with our proposal compared with results obtained with other techniques [1-2].

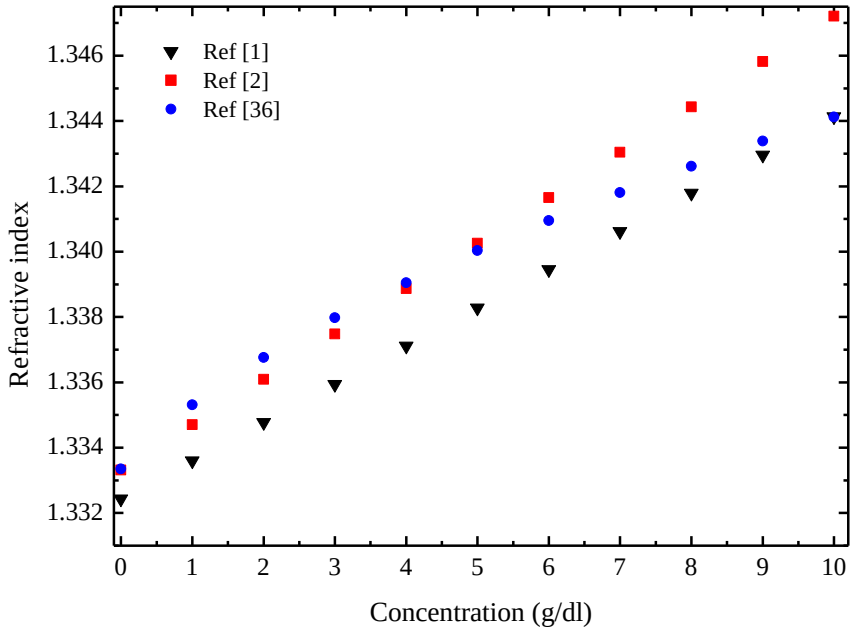

Fig. 13 Comparative graph of the refractive index as a function of glucose concentration obtained with different techniques [1-2, 36]

Fig. 13 shows the corresponding values of the refractive index as a function of concentration. The triangles correspond to values that were obtained with an interferometry technique [1], the squares are the values reported in a chemical handbook [2] and circles are the values obtained with the technique reported here. In Fig. 13 it can be seen the behavior of the refractive index in a range between 0 and 10 g/dl as reported by Refs. [1] and [2]. Although the values from Refs. [1] and [2] are similar to the results obtained with our

proposal, by careful observing the behavior of the plots, on can notice linear responses. As we have shown in our analytical approach, the response in this range can not be linear. Now, with our analytical result, it is possible to ascertain the correctness of the measurements. In our case, our technique gives enough accuracy as to match with the theoretical prediction.

In chapter four we extend our technique for the measurements of glucose concentration in turbid media.

Chapter 4

Experimental results for turbid media

In this chapter we describe the experimental results to measure glucose concentration in a turbid sample that simulates optical scattering properties of biological tissues. First, we describe how the turbid samples were prepared. Then, we describe the experimental process of the measurements for 600 and 300 lines/mm gratings and the results obtained. Finally, we give our results for a real biological tissue.

4.1 Turbid sample preparation

Phantoms made with Intralipid^{MR} suspension are commonly used for experiments that simulate optical properties of biological tissues [19-21] as the anisotropy coefficient (g), scattering coefficient (μ_s), reduced scattering coefficient (μ_s') and absorption coefficient (μ_A) are basically similar as illustrated numerically in table 4.. The concentrations of these phantoms are around of 1 to 2% of Intralipid ^{MR} concentration. The sample prepared here has a higher concentration (2.5%) to demonstrate the usefulness of our technique. This concentration gives the optical properties of the human breast and skin tissue [37, 38]. Approximate values of the optical parameters of the phantoms in the range between 0.5 and 2.5 % of Intralipid ^{MR} are given in table 4.

Our experiments were conducted by using an Intralipid^{MR} from 20% stock commercially available solved in tri-distilled water.

Intralipid [MR] concentration (%)	Scattering coefficient μ_s (cm^{-1})	Reduced scattering coefficient μ_s' (cm^{-1})	Anisotropy coefficient g	Absorption coefficient μ_A (cm^{-1})
0.5	5.0	1.0	0.8	0.6
1.0	12.0	2.5	0.8	0.6
1.5	20.0	4.0	0.8	0.7
2.0	30.0	6.0	0.8	0.7
2.5	40.0	8.0	0.8	0.75

Table 4 Intralipid [MR] concentrations between 0.5 and 2.5 % and their corresponding optical parameters estimated from [37-38, 39]

Our base sample consists in a 2.5 % Intralipid [MR] solution without glucose. For brevity, this sample henceforth will be referred as the zero glucose concentration or 0 mg/dl. The base sample with Intralipid[MR] was measured again using the two gratings used in the last section. The glucose concentration was obtained from a glucose patron based on Dextrose Anhydrous commercially available as in our above description.

The solutions were prepared as follows,

(a) For concentrations between 0 and 1.0 g/dl with the 600 lines/mm grating we took a recipient in which we poured 100 ml of 2.5% Intralipid [MR] solution without glucose, this was our base sample. Then in other recipient we poured again 100 ml of 2.5% Intralipid [MR] solution, but this time we add noun amounts of glucose in steps of 0.25 g/dl to obtain the glucose concentration desired.

(b) For the 300 lines/mm grating we repeated the same procedure refer in point (a). The glucose added to the solution was in steps of 1.5 g/dl to obtain concentrations between 0 and 7.5 g/dl.

Table 5 summarizes the samples prepared for the 600 and 300 lines/mm gratings.

Intralipid ^{MR} Samples of glucose concentration for Λ_{600} (g/dl)	Intralipid ^{MR} Samples of glucose concentration (g/dl) Λ_{300} (g/dl)
0	0
0.25	1.5
0.50	3.0
0.75	4.5
1.00	6.0
-	7.5

Table 5 Experimental Intralipid ^{MR} samples prepared for both gratings 600 and 300 lines/mm [40].

In the next section we describe the experimental procedure to measure glucose in a turbid medium.

4.2 Experimental procedure

For each grating the experimental process was as follows,

- First, the system was adjusted to the best focusing conditions with the sample of zero glucose concentration.
- Second, a region of the grating was scanned and recorded.
- After that, a know amount of glucose concentration was poured into the container with Intralipid ^{MR} solution and was left to settle.
- Then, the same region of the grating was scanned and recorded.
- Finally, we repeated the same process for each new glucose concentration.

We verify the repeatability of the measurements by scanning several times the same region. In each scan 200 pixels were recorded. All measurements were made a temperature constant of 25º C. Each measurement took approximately one minute.

4.3 Experimental results for 600 lines/mm grating

For measurements between 0 and 1.0 g/dl we used the 600 lines/mm grating. Fig. 14 shows a plot of the reflection profile of the grating recorded by the system for different glucose concentration. The plot of zero glucose concentration has been normalized.

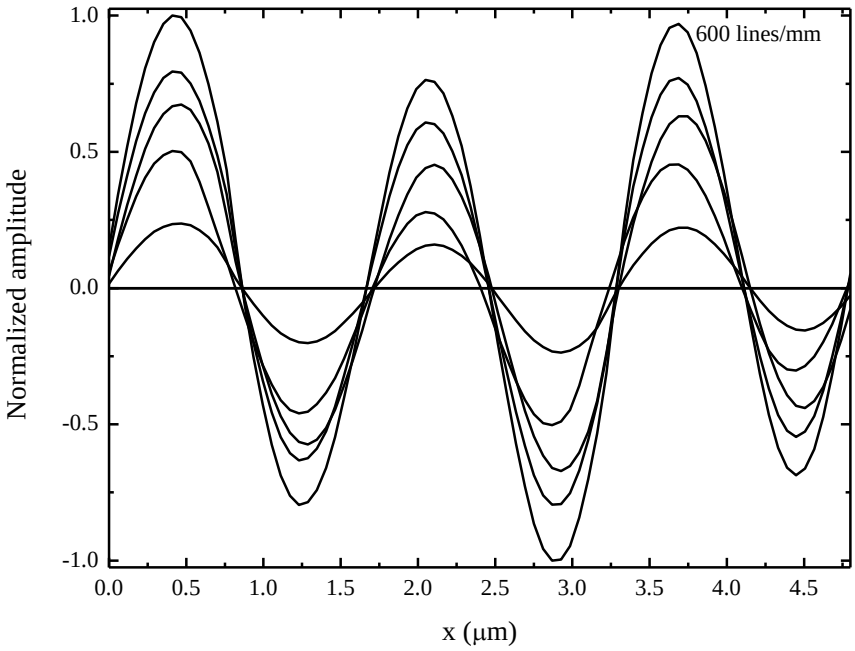

Fig.14 Experimental normalized vertical amplitude for 600 lines/mm grating for the turbid medium. In the figure small amplitudes correspond to higher concentrations

Fig. 15 shows a plot of the of the experimental rms values for the recorded vertical heights as a function of c. The solid line represents the fitted linear curves given by Eq. (29)

$$rms_{600} = -0.2910\ c + 0.7214, \tag{29}$$

where rms_{600} is the rms values of the profiles for 600 lines/mm grating and c is the glucose concentration given in g/dl.

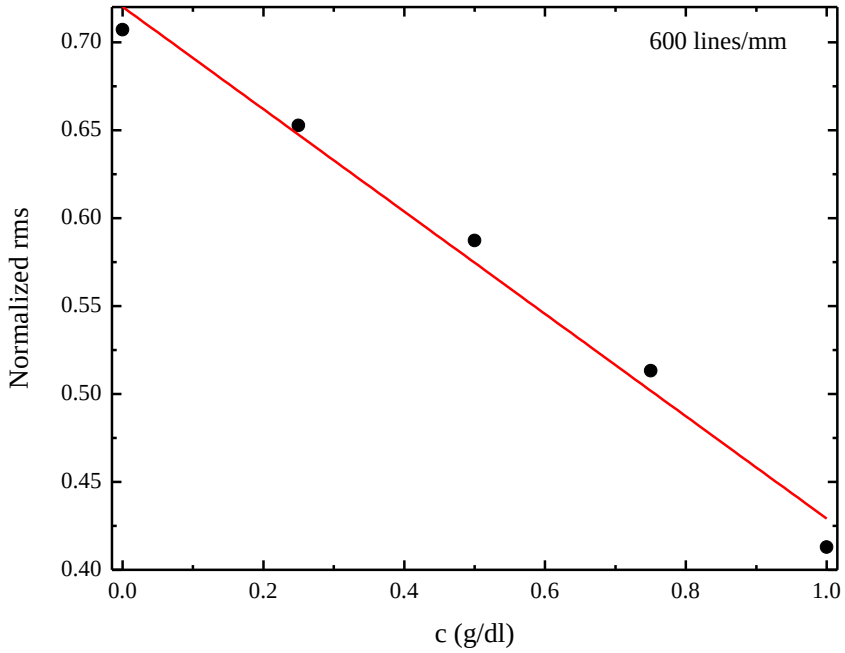

Fig.15 Plot of the rms values of the normalized vertical heights of the normalized vertical profiles for 600 lines/mm grating as a function of glucose concentration

In the next section we give the experimental results for the 300 lines/mm grating.

4.4 Experimental result for the 300 lines/mm grating

For measure concentrations between 0 and 7.5 g/dl we used the 300 lines/mm grating. Fig. 16 depicts the vertical profiles measured. Again, smaller amplitudes correspond to higher concentrations. The plot of zero glucose concentration has been normalized.

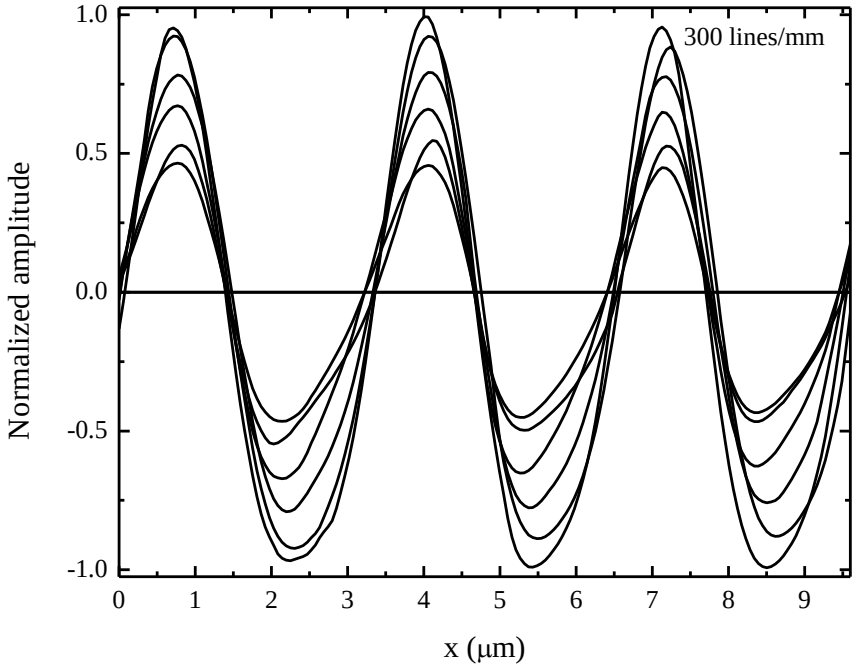

Fig.16 Experimental normalized vertical amplitude for 300 lines/mm grating for the turbid medium. In the figure small amplitudes correspond to higher concentrations

A plot of the rms values as a function of c obtained can be found in Fig. 17. The plot includes the fitted linear curve depicted by a solid line. Eq. (30) represents the fitted curve.

$$rms_{300} = -0.0559\ c + 0.7195, \tag{30}$$

where rms_{300} is the rms values of the profiles for 300 lines/mm grating and c is the glucose concentration given in g/dl.

According to table I a non-linear response between the detected power and c is obtained for the transparent medium in contrast to the case of the turbid medium as stated by Eqs. (29) and (30). This is due to scattering which highly widens the beam. Thus, changes in c will induce very small relative changes in r_0 compared with the transparent case. Graphically, this corresponds to a very small region of the plot of Fig. 6 around a large value of r_0 giving a linear response.

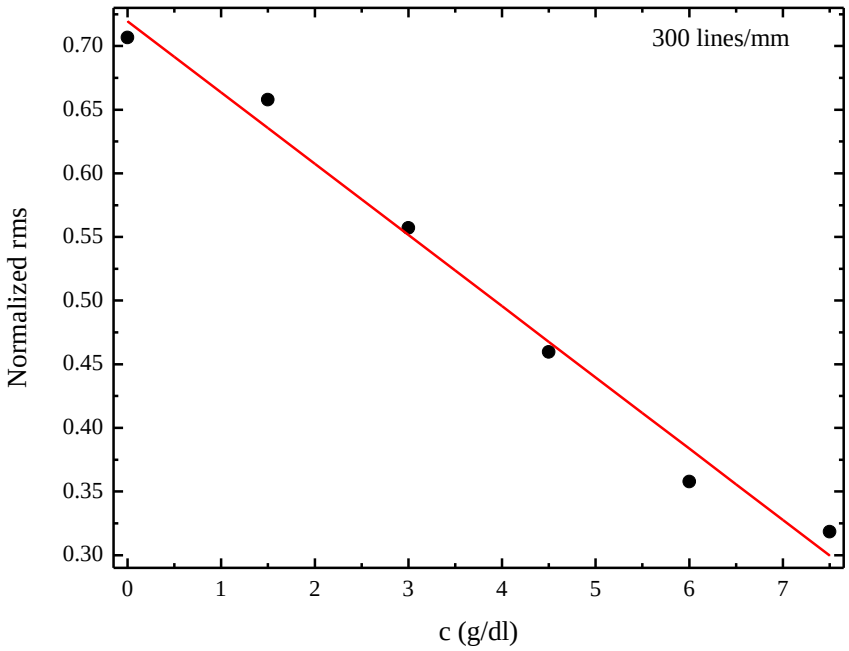

Fig.17 Plot of the rms values of the normalized vertical heights of the normalized vertical profiles for 300 lines/mm grating as a function of glucose concentration.

Although the signal obtained is very small compared with the case of the transparent sample the KED has a very high sensitivity making it appropriate to perform the detection of glucose concentration.

4.5 Experimental results for real biological tissue

To show the potential application of our proposal we proof our system we a real biological tissue. The biological tissue consists in a small piece of chicken skin which was taken of its leg with a geometrical thickness of approximately of 1 mm. The optical parameters of the chicken skin based in [41] are within the following ranges: $10.85 < \mu_s' < 21.42$ cm^{-1}, $0.16 < \mu_a < 0.59$ cm^{-1} and $0.7 < g < 0.9$.

To perform our experiment the sample was placed in the optical path of the light as depicted in Fig. 1. A plot of profile of the grating recorded through the skin-sample is show in Fig. 17. Furthermore, we compared the same region of the grating when we used other solutions as tri-distilled water, and different Intralipid ^{MR} concentrations between 1.5 and

2.5 %. In order to have a one-to-one comparison, we set the attenuator to appropriate conditions to get the approximately the same vertical heights. In Fig. 18 is shown some undesirable features on the profile obtained with the chicken skin sample due to highly scattered beam.

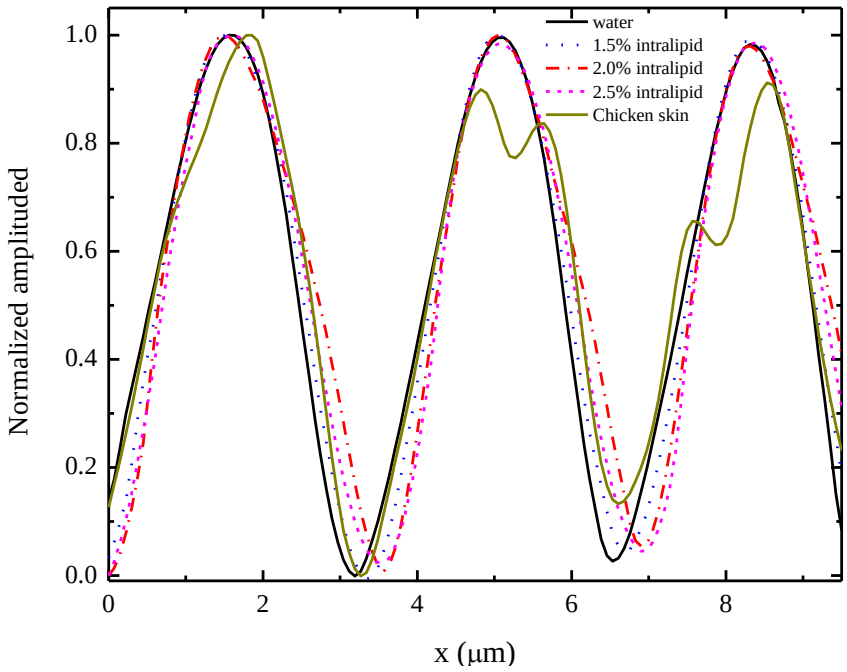

Fig. 18 Comparison of the grating profile recorded with the KED for a chicken skin-sample compared with samples of pure water and different Intralipid [MR] concentrations.

Due to we used a laser with a available power of 3 mW; we perform the experiment with the 300 lines/mm grating. With this power available was not possible to obtain the profile with the 600 lines/mm grating. We found experimentally that for a 5 mm sample width, a concentration of 3% of Intralipid [MR] is the upper limit that allows us detecting the grating profile. Using higher power and/or infrared light should enhance the penetration depth.

It is important to remark that our proposal requires calibrating the system with a sample of zero glucose concentration before performing the measurements. This limitation can possibly be overcome taking advantage that the system has a linear response as a function of glucose concentration, being independent of the scattering and absorption properties of the medium. Thus, if a relationship of the optical properties between different

media could be obtained by other means, it would be sufficient to calibrate only one medium; future research in this direction is necessary, taking into account the length of the turbid media.

Chapter 5

Conclusions

In this dissertation we have described an optical technique that allows classifying liquid solutions by analyzing the semi-width of a single Gaussian beam transmitted by the sample while profiling a commercially available calibrated reflective grating by means of the homodyne knife-edge detector which has been devised here in Centro de Investigaciones en Óptica. The homodyne detector exhibited high sensitivity to allow us measuring with high precision the profile of a calibrated reflective grating which in turn allows us to accurately determine the change in the semi-width of the beam transmitted thorough the sample. In this way we achieve to obtain plots of glucose concentration as a function of the index of refraction of the samples.

Furthermore, we have shown how a single Gaussian probe beam carries enough information of the physical phenomenon to allow us to give a general classification of the concentration of transparent solutions.

We extended our technique for measuring glucose concentration in turbid media samples that simulates optical properties of biological. For the moment being our theory is limited to solutions whose refractive index increases with concentration.

Our technique exhibited sensitivity high enough to allow us to provide evidence on the applicability of our technique with a real biological tissue. We showed that, although the biological tissue is highly dispersive, the system is still capable of recording the grating profile of the calibrated grating with reasonable accuracy, making it apparent the usefulness of our technique for the case of biological samples. It is important to remark that for the case of real biological samples it still remains the necessity of finding a method that allows us to calibrate the system if the sample under test is an unknown one. More research is necessary in this direction.

6. Bibliography

[1] Y. L. Yeh, "Real-time measurement of glucose concentration and average refractive index using a laser interferometer," Opt. Lasers Eng. **46**, 666-670 (2008).

[2] Weast RC. CRC handbook of chemistry and physics, 61st. Boca Raton, FL: CRC Press, Inc; 1980.

[3] Kirill V. Larin, Taner Akkin, Rinat O. Esenaliev, Massoud Motamedi, and Thomas E. Milner, "Phase-Sensitive Optical Low-Coherence Reflectometry for the Detection of Analyte Concentrations," Appl. Opt. **43**, 3408-3414 (2004).

[4] Y. Liu, P. Hering, and M. O. Scully, Appl. Phys. B **54**, 18 (1992).

[5] W. Mahmood bin Mat Yunus and Azizan bin Abdul Rahman, "Refractive index of solutions at high concentrations," Appl. Opt. 27, 3341-3343 (1988).

[6] Chiao-Ling Wong, Chien-Chang Huang, Wei-Bin Lu, Wen-Ming Chen, Jo-Shu Chang, “Producing 2,3-butanediol from agricultural waste using an indigenous Klebsiella sp. Zmd30 strain”, Biochemical Engineering Journal, **69**, 32-40 (2012)

[7] Yang, T.W., Rao, Z.M., Zhang, X., Lin, Q., Xia, H.F., Xu, Z.H., Yang, S.T., “Production of 2,3-butanediol from glucose by GRAS microorganism Bacillus amyloliquefaciens.” J. Basic Microbiol. **51**, 650–658 (2011)

[8]Lee J Y and S. K. Tsai, “Measurement of refractive index variation of liquids by surface Plasmon resonance and wavelength-modulated heterodyne interferometry,” Opt. Commun. **284**, 925-929 (2011).

[9] Chen K, Hsu C; Su, D.-C, “Interferometric optical sensor for measuring glucose concentration,” Appl. Opt. **42**, 5774–5776 (2003).

[10] M. Chiu, S. Wand, and R. Chang, “D-type biosensor based on surface-plasmon resonance technology and heterodyne interferometry,” Opt. Lett. **30**, 233–235 (2005).

[11] K. H. Chen, J.-H. Chen, S.-W. Kuo, T.-T. Kuo, and M.-H. Lai, "Non-contact method for measuring solution concentration using surface plasmon resonance apparatus and heterodyne interferometry," Opt. Commun. **283**, 2812-2185 (2010).

[12] Wang C, Kaya M, Wang C; "Evanescent field-fiber loop ringdown glucose sensor," J. Biomed. Opt. **17**(3) (2012).

[13] T. Q. Lin, Y. L. Lu, C. C. Hsu, “Fabrication of glucose fiber sensor based on immobilized GOD technique for rapid measurement,” Opt. Express. **26**, 27560 –27566 (2010).

[14] M. L. Dong, K. G. Goyal, B. W. Worth, S. S. Makkar, W. R. Calhourn, L. M. Bali, and S. Bali, J. Biomed, “Accurate in situ measurement of complex refractive index and particle size in intralipid emulsions” Opt. **18**, 087003 (2013)

[15] Q. Ye et al., “Measurement of the complex refractive index of tissue-mimicking phantoms and biotissue by extended differential total reflection method,” J. Biomed. Opt. **16(9)**, 097001 (2011)

[16] P. Di Ninni, F. Martelli, and G. Zaccanti, “Intralipid: towards a diffusive reference standard for optical tissue phantoms,” Phys. Med. Biol. **56(2)**, N21–N28 (2011).

[17] R. Michels, F. Foschum, and A. Kienle, “Optical properties of fat emulsions,” Opt. Express **16(8)**, 5907–5925, (2008)

[18] Ding H, Lu J Q, Jacobs K M and Hu X. H., "Determination of refractive indices of porcine skin tissues and Intralipid ateight wavelengths between 325 and 1557 nm," J. Opt. Soc. Am. A **22,** 1151–7, (2005)

[19] K. Jakobsohn, M. Motiei, M. Sinvani, R. Popovtzer, "Towards real-time detection of tumor margins using photothermal imaging of immune-targeted gold nanoparticles," Int. J. Nanomedicine, **7**, 4707–471, (2012)

[20] Canpolat, "Variation of photon density distribution with system component within Intralipid emulsion"; M. Optik (Munich, Ger.), **122**, 887–890, (2011)

[21] Dam J. S. , , Pedersn C. B. , , Dalgaard T. , , Fabricius P. A. , , Aruna P. , , and Engles S Anderson , " Fiber optic probe for noninvasive real-time determination of tissue optical properties at multiple wavelengths," Appl. Opt. , **40**, (7), 1155–1164, (2001)

[22] M. Kirillin, A. Priezzhev, M. Kinnunen, E. Alarousu, Z. Zhao, J. Hast, and R. Myllylä, "Glucose sensing in aqueous IntralipidTM suspension with an optical coherence tomography system: experiment and Monte Carlo simulation", in Optical Diagnostics and Sensing IV, edited by A. Priezzhev, G. Cote, Proceedings of SPIE Vol. **5325**, SPIE Press, Bellingham, 164-174 (2004).

[23] Larin K. V., , Ashitkov T. V., , Larina I., , Petrova I., , Eledrisi M., , Motamedi M., , and Esenaliev R. O., " Optical coherence tomography and noninvasive blood glucose monitoring: a review," Proc. SPIE. **0277**-786X 5474, , 285–290 (2004)

[24]K. Larin, I. Larina, M. Motamedi, V. Gelikonov, R. Kuranov, and R. Esenaliev, "Potential application of optical coherence tomography for non-invasive monitoring of glucose concentration," Proc SPIE INT SOC OPT ENG., **4263**, pp. 83-90, (2001)

[25] Erkki Alarousu, Jukka Hast, Matti Kinnunen, Mikhail Kirillin, Risto Myllyla, Jerzy Plucinski, Alexey Popov, Alexander Priezzhev, Tuukka Prykari, Juha Saarela, and Zuomin

Zhao, “Non-invasive glucose sensing in scattering media using OCT, PAS and TOF techniques,” Proc SPIE **5474-05**, (2004)

[26] A.A. Zanishevskaya, A.V. Malinin, Yu.S. Skibina, V.V. Tuchin, M.V. Chainikov, V.I. Beloglazov, I.Yu. Silokhin, A.M. Ermakova, “Determination of glucose concentration in biological liquids using photonic crystal waveguides,” Optika i Spektroskopiya, **115**, No. 2, 266–271, (2013)

[27] Kafidova, G.A., Aksenov, E. T. and Petrov, V.M., "Measurement of glucose concentration in turbid media by the polarization state of backscattered laser light," Proc. SPIE **8803**, 880306 (2013)

[28] Daniel Côté, I. Alex Vitkin, “Robust concentration determination of optically active molecules in turbid media with validated three-dimensional polarization sensitive Monte Carlo calculations,” Opt. Express **13**, 148-163, (2005)

[29] Z. Zhao, “Pulsed photoacoustic techniques and glucose determination in human blood and tissue,” Ph.D. thesis (University of Oulu, 2002).

[30] Kottmann J., Rey J. M., Luginbühl J., Reichmann E., Sigrist M. W., “Glucose sensing in human epidermis using mid-infrared photoacoustic detection,” Biomed. Opt. Express **3(4)**, 667–680 (2012)

[31] K. Larin and A. Oraevsky, "Optoacoustic signal profiles for monitoring glucose concentration in turbid media," Proc. SPIE, **3726**, 576-563, (1998)

[32] Raju Poddar, Joseph Tomas Andrews, Pratyoosh Shukla, Pratima Sen, “Noninvasive glucose monitoring techniques: a review and current trends”, Medical Physics, Instrumentation and Detectors (2008), arXiv:0810.5755v1 [physics.med-ph] http://eprint arxiv:0810.5755

[33] Spiegel, Murray R. Mathematical Handbook of formulas and Tables, 2/1999a.Ed-McGraw-Hill

[34] M. Cywiak, J. Murakowski, G. Wade,, "Beam Blocking Method for Optical Characterization of Surfaces", Int J Imaging Syst Technol, **11**, 164–169, (2000).

[35] Murakowski J; Cywiak M; Rosner B; and van der Weide, D, "Far field optical imaging with subwavelength resolution," Opt. Comm., **185**, 295-303 (2000).

[36] Joel Cervantes-L, Moisés Cywiak, Octavio Olvera-R, Arquímedes Morales; "Defocusing properties of Gaussian beams for measuring refractive index of thin transparent samples," Opt. Comm., **309**, 108-113 (2013)

[37] Homa Assadi, Rafii Karshafian, Alexandre Douplik, "Optical scattering properties of intralipid phantom in presence of encapsulated microbubbles," International Journal of Photoenergy, Novel Photomedicine Issue, (2014)

[38] Sandell J L and Zhu T C, "A review of in-vivo optical properties of human tissues and its impact on PDT," J. Biophotonics, **4**, 773–87, (2011)

[39] Aernouts, B., Zamora-Rojas, E., Van Beers, R., Watté, R., Wang, L., Tsuta, M., & Saeys, W. "Supercontinuum laser based optical characterization of Intralipid® phantoms in the 500-2250 nm range," Optics Express, **21**(26), 32450-32467, (2013)

[40] Joel Cervantes-L, Moisés Cywiak, Octavio Olvera-R, David Cywiak; "Measurement of glucose concentration in a thin turbid medium by a transmitted Gaussian beam," Opt. Comm., **331**, 239-243 (2014)

[41] Singh, A., Karsten, A. E. and Dam, J. S., "Robustness and accuracy of the calibration model for the determination of the optical properties of chicken skin," Proceedings of the International Conference of the World Association of Laser Therapy, 165-169 (2008)

Appendix A

Related publications

In this appendix we add the publications made during the doctoral stay.

A1 Joel Cervantes-L, Moisés Cywiak, Octavio Olvera-R, Arquímedes Morales; "Defocusing properties of Gaussian beams for measuring refractive index of thin transparent samples," Opt. Comm., **309**, 108-113 (2013)

A2 Joel Cervantes-L, Moisés Cywiak, Octavio Olvera-R, David Cywiak; "Measurement of glucose concentration in a thin turbid medium by a transmitted Gaussian beam," Opt. Comm., **331**, 239-243 (2014)

A3 Octavio Olvera-R, Moisés Cywiak, **Joel Cervantes-L**, and Arquímedes Morales, "Refractive index and geometrical thickness measurement of a transparent pellicle in air by Gaussian beam defocusing," Appl. Opt. **53**, 2267-2272 (2014)

A4 Octavio Olvera-R, Moisés Cywiak, **Joel Cervantes-L**, and , David Cywiak; "Refractive index and geometrical thickness measurement of thin optical samples by a transmitted Gaussian beam," ppl. Opt. **30**, (under press 2014)

Optics Communications 309 (2013) 108–113

Contents lists available at SciVerse ScienceDirect

Optics Communications

journal homepage: www.elsevier.com/locate/optcom

Defocusing properties of Gaussian beams for measuring refractive index of thin transparent samples

Joel Cervantes-L, Moisés Cywiak*, Octavio Olvera-R, Arquímedes Morales

Centro de Investigaciones en Óptica A. C., León Gto., Leon, Guanajuato 37150, Mexico

ARTICLE INFO

Article history:
Received 31 May 2013
Accepted 3 July 2013
Available online 17 July 2013

Keywords:
Holographic gratings
Homodyne detection
Glucose concentration
Gaussian beams

ABSTRACT

We show how the defocusing properties of Gaussian beams can be used to measure the refractive index of solutions in thin transparent samples (less than 2 mm). Additionally, it is possible to predict analytically the shape of the plot for the refractive index as a function of concentration in any range. Our theory is limited for substances whose refractive index increases with concentration. The thin sample is placed between the focusing lens and its back focal plane and the system is adjusted to best focusing conditions. As a result, changes of the refractive index of the sample cause variations of the size of the focused beam. To measure with high accuracy the size of the beam we use the homodyne knife-edge profilometer while profiling a calibrated holographic reflective grating. The recorded vertical heights of the grating provide statistical data for improving even more the accuracy of the measurements. We demonstrate that the sensitivity of the system is a function of the pitch of the grating allowing selecting the range of interest. We apply our method for glucose liquid solutions. We include analytical description of our method and experimental results.

1. Introduction

Calculating accurately the refractive index of solutions is of major importance. Additionally, it is very significant to accurately know the analytical dependence of the refractive index as a function of concentration. However, for the best of our knowledge the techniques reported relay only in describing the methodology of the measurements and the corresponding range of applicability and there is no an analytical model which may be used to predict physically the peculiar shape that exhibits the plot of the refractive index as a function of concentration for liquid solutions. Moreover, by reviewing the literature one can find discrepancies of the reported plots, especially for glucose [1–5]. Then, although the method reported here can be applied to any transparent substance, we concentrate our experimental section to the case of glucose in thin liquid samples due to its inherent importance.

Glucose measuring techniques may be divided into two ranges, high and low concentrations. Low concentration techniques that are necessary for the satisfactory production of 2,3-BDO using DNS and GRAS methods can be found in [6,7]. To measure low glucose concentration elaborated techniques must be applied; for example surface-plasmon resonance (SPR) [8–11] and fiber optics techniques [12,13]. The referred techniques require large samples and, as mentioned, are focused solely in describing the measurements and the range of applicability, therefore an overall physical model cannot be inferred. In what follows we describe how our theory is applied for measuring refractive index as a function of glucose concentration and we show how it can be applied to give an overall description of the behavior.

2. Analytical description

2.1. Gaussian beam propagation

To analyze our proposal we will refer to Fig. 1 in which a Gaussian beam emerging from a laser of wavelength λ, focused by a lens at its back focal plane is depicted. The thin sample is placed in the optical path. The width of the sample is exaggerated in the drawing for the description. For simplicity and without loss of generality our calculations are one-dimensional. The overall propagation consists of six propagations. First, the beam is propagated a distance z_0 towards the focusing lens and a focusing quadratic phase due to the lens is introduced. Second, the convergent beam is propagated a distance z_1 just before the left face of the container. Third, the light propagates inside the glass a distance z_2 with a refractive index n. Fourth, the beam travels through the solution a distance z_3 in a medium with a refractive index n_S. Fifth, the light propagates inside the glass with a refractive index n a distance z_4. Finally, the beam propagates a distance z_5 up to the back focal plane.

* Corresponding author. Tel.: +52 477 4414200.
E-mail address: moi@cio.mx (M. Cywiak).

0030-4018/$ - see front matter © 2013 Published by Elsevier B.V.
http://dx.doi.org/10.1016/j.optcom.2013.07.007

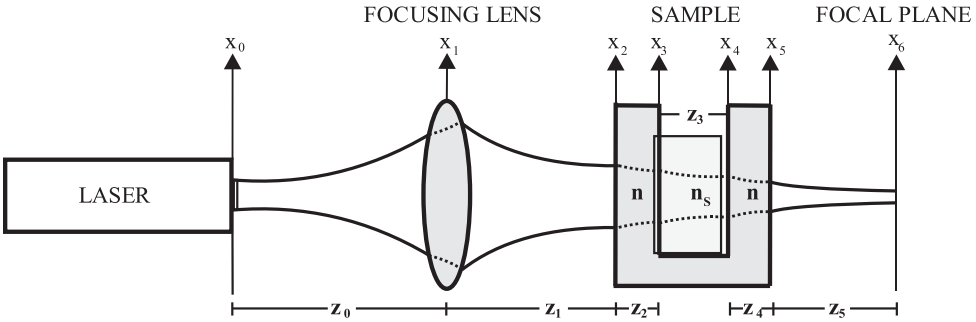

Fig. 1. Schematic representation of the Gaussian beam propagation.

To simplify the calculations we consider that the focusing lens is an ideal one, so it only introduces a quadratic phase and it is placed at the vertical axis, x_1.

For a more realistic modeling we are considering the width of the glass walls of the container as follows. x_2 and x_3 are the axes of the left wall (outer and inner faces, respectively); x_4 and x_5 will refer to the right wall (inner and outer, respectively). x_6 is the coordinate at the focal plane.

The Gaussian beam distribution at the output of the laser at x_0 can be represented as,

$$\Psi_0(x_0) = A_0 \exp\left(-\frac{x_0^2}{r_0^2}\right), \tag{1}$$

where A_0 is a constant amplitude and the exponential gives the Gaussian behavior; r_0 is the beam semi-width and x_0 represents the coordinate of the plane at the output of the laser.

The field distribution at plane x_1, just before reaching the lens, is calculated using the Fresnel diffraction integral as follows,

$$\Psi_1(x_1) = \frac{\exp(i\,2\pi\, z_0/\lambda)}{\sqrt{i\lambda\, z_0}} \int_{-\infty}^{\infty} A_0 \exp\left(-\frac{x_0^2}{r_0^2}\right) \exp\left[\frac{i\,\pi}{\lambda\, z_0}(x_0 - x_1)^2\right] dx_0. \tag{2}$$

Eq. (2) can be solved exactly obtaining

$$\Psi_1(x_1) = A_1 \exp\left(-\frac{x_1^2}{r_1^2}\right) \exp(i\,\beta_1 x_1^2), \tag{3}$$

where,

$$A_1 = \frac{\exp(i\,2\pi\, z_0/\lambda)}{\sqrt{i\lambda\, z_0}} \sqrt{\frac{\pi\, r_0^2\, \lambda\, z_0}{\lambda\, z_0 - i\pi\, r_0^2}}, \tag{4a}$$

$$r_1 = \frac{\sqrt{\lambda^2\, z_0^2 + \pi^2\, r_0^4}}{\pi\, r_0}, \tag{4b}$$

$$\beta_1 = \frac{\pi}{\lambda\, z_0}\left(1 - \frac{\pi^2\, r_0^4}{\lambda^2\, z_0^2 + \pi^2\, r_0^4}\right). \tag{4c}$$

In the above equations A_1 represents the complex amplitude of the beam at the left of the lens (just before reaching the lens). r_1 is the semi-width of the beam. β_1 is the constant in the quadratic phase of Eq. (3) that in this case is divergent.

In order to calculate the subsequent propagations straightforwardly, we notice that the set of Eqs. (4a)–(4c) can be used recursively. Before doing this, the quadratic phase of the lens has to be considered. Thus, β_1 has to be updated as $\beta_1 - \pi/\lambda f$, being f the focal length of the lens.

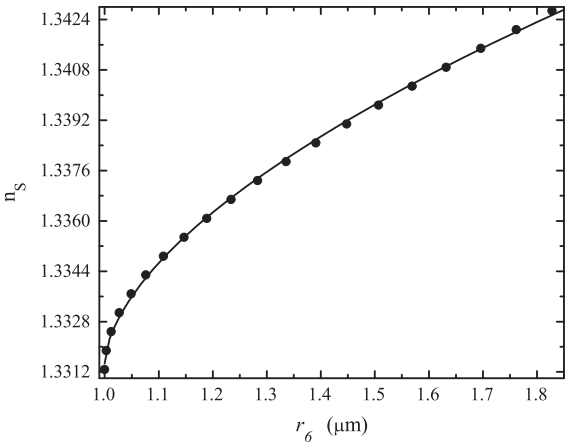

Fig. 2. n_S as a function of r_6. Dots correspond to calculations obtained by diffraction. The solid line is the fitted curve.

Using the recursive set of equations we obtain for the semi-width up to the back focal plane

$$r_6 = \frac{\sqrt{\lambda^2\, z_5^2 + r_5^4(\beta_5\, \lambda\, z_5 + \pi)^2}}{\pi\, r_5}. \tag{5}$$

In Eq. (5) β_5 and r_5 have to be calculated by their preceding values.

To apply the above equations to our system we now calculate the best focusing conditions that correspond to the minimum possible value of r_6. For this, the value of z_5 is varied in a narrow vicinity around the back focal plane until r_6 reaches a minimum which in our case is set to 1 μm to match with our experimental setup. To perform these calculations we used $z_3 = 1.2$ mm and $\lambda = 632.8$ nm. Our initial condition corresponds to zero glucose concentration consisting of purely tri-distilled water at 25 °C with a refractive index of 1.3312 which is known by other means.

Once adjusted our theoretical system, with the above equations we tabulated n_s against r_6.

It is possible to fit an equation to the tabulated data. We find,

$$n_S = 1.3313 + 41.84(r_6 - 1 \times 10^{-6})^{0.5881} \tag{6}$$

where n_S stands for the refractive index of the solution. Fig. 2 shows a plot of the tabulated data (dots) and the fitted by Eq. (6) (solid line).

Fig. 2 is the key of our defocusing proposal. It reveals an important physical effect. Around the optimal focusing conditions (in our case to $r_6 = 1$ μm, $n_S = 1.3312$) large variations of n_S result in small variations of r_6. This is because the size of the Gaussian beam remains approximately collimated over the beam waist region which corresponds to the Rayleigh range. Further increments of the refractive index cause larger variations of the

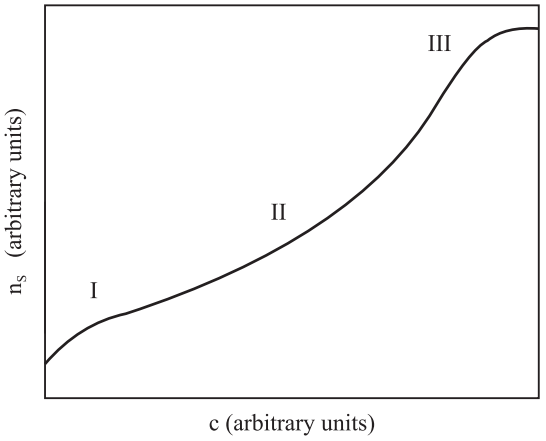

Fig. 3. Qualitative n_S as a function of c for a hypothetical solution as described in the text.

semi-width now outside the Rayleigh range. The plot of Fig. 2 resides in the Rayleigh region and extends into a small region outside it.

It is now necessary to find how the refractive index is related to the concentration of the solution, which hereafter will be denoted as c. For this we first find qualitatively how $c$depends on r_6. We will limit our discussion to substances where n_s increases with c, as follows.

First, when the concentration is low, it is reasonable to expect linearity between c and r_6. Increments of c will only cause small increments of r_6 as we reside into the Rayleigh region. Further increasing c, at this time outside the Rayleigh region, will cause larger increments of r_6 (now not necessarily linear), until the solution approaches saturation which will cause r_6 to approach asymptotically to a certain finite value. This physical behavior can be represented by three regions which we denote accordingly as the Rayleigh region, the free region and the saturation region or equivalently regions I, II and III.

For each region it is possible to propose qualitatively a relation of r_6 as a function of c. This relation is to be substituted in Eq. (6). In Fig. 3 we show qualitatively the shape of the expected plot for a hypothetical solution which includes the three regions.

To demonstrate experimentally our previous theory we performed measurements with glucose solutions at low concentrations (less than 10 g/dl or equivalently less than 10%), falling in a small vicinity between regions I and II. Additionally, as we are in a region of low concentration we expect a linear dependence of r_6 against c of the form,

$$r_6(c) = K_1 + K_2\, c, \tag{7}$$

where the positive constant values K_m, $m = 1,2$ must be determined experimentally for each particular substance. In our experimental section we verify this assertion.

In our experiments, the semi-width has to be measured with high accuracy, thus, we take advantage of the homodyne knife edge detector (KED) which results appropriate for our purposes. For convenience the KED is briefly described in the next subsection.

2.2. Homodyne knife-edge detector for measuring the semi-width variations

In this subsection, we show how the KED [14,15] is used to perform the detection of the semi-width of the focused beam to measure glucose concentration. The setup is illustrated in Fig. 4.

A polarized He–Ne laser beam ($\lambda = 632\ nm$) is focused on the surface under test (SUT) which in our case is a calibrated holographic reflective grating. The focusing lens (L) is a $100\times$ microscope objective with a working distance of 1 cm allowing the properly placement of the sample. The probe beam, reflected by the grating, is sent for detection by means of a beam splitter (BS) to a half-blocked photodiode. As depicted in Fig. 4 the sample is placed between the focusing lens and the SUT, in concordance with Fig. 1. An attenuator (A) is included to avoid damaging the grating due to excessive heating. A flexure mode piezoelectric transducer (PZT) vibrates the grating at approximately 10 Hz with small amplitude δ_0 in the x-direction as depicted and it is also used to mechanically scan the grating at a slow rate in the same direction. A lock-in amplifier is used to generate the vibration and to detect the AC signal from the photodiode. A personal computer (PC) adds the scanning signal and communicates with the lock-in by GPIB to automate the measurements.

The walls of the glass container should be parallel to avoid some deflection of the beam that can slightly affect the measurements. For this purpose, we constructed containers made of thin glass (0.13 mm), with dimensions $5.0\times 5.0\times 1.2\ mm^3$, where the light path is along the 1.2 mm width. One advantage of our proposal is that the system can work with small samples however as a preliminary experiment our container is large because it was handmade.

As shown in [14,15], the AC power collected by the half-blocked photodiode is given by,

$$P_{out}(x_6,y_6) = -i\frac{8P_0}{\lambda r_6^2}\delta_0 \int_{-\infty}^{\infty}\int_{-\infty}^{\infty} \exp\left(-2\frac{(x-x_6)^2+(y-y_6)^2}{r_6^2}\right) \times erf\left(i\frac{x-x_6}{r_6}\right)\ \frac{\partial}{\partial x}h(x,y)\ dx\ dy, \tag{8}$$

where $h(x_6,y_6)$ represents the profile of the SUT considered in a plane (x_6,y_6). This coordinates are chosen to be compatible with Fig. 1. P_0 is the beam power which is constant. The semi-width of the Gaussian probe beam (r_6) is focused at (x_6,y_6). In Eq. (8) the partial derivative of the height distribution appears as a consequence of a first order expansion due to the vibration of the SUT with small amplitude δ_0 as described in [14,15]. $erf()$ is the error function and $i=\sqrt{-1}$. The parameters x,y are meaningless and are used solely for the integration.

The integral in Eq. (8) represents the convolution of two functions. One function is the derivative of the vertical height distribution of the SUT. The second function is the impulse response of the system, namely,

$$\Re(x_6,y_6) = -i\frac{8P_0\delta_0}{\lambda r_6^2}\ exp\ \left(-2\frac{x_6^2+y_6^2}{r_6^2}\right)\ erf\left(i\frac{x_6}{r_6}\right)\ . \tag{9}$$

Eq. (8) will now be used to describe the behavior of the output power as a function of defocus when profiling a sinusoidal reflective grating. In this case, $h(x,y)$ can be expressed as

$$h(x,y) = h_0\left[1+\ \sin\left(\frac{2\pi}{\Lambda}x\right)\right], \tag{10}$$

where Λ is the period in the x-direction and h_0 is the height amplitude of the grating. After performing the integral given in Eq. (8), we obtain the detected power as,

$$P_{out}(x_6,y_6) = \frac{8\pi^2\delta_0}{\lambda\Lambda}P_0\ exp\left(-\frac{\pi^2 r_6^2}{2\Lambda^2}\right)erf\left(\frac{\pi\, r_6}{\sqrt{2}\Lambda}\right)\left[h_0\sin\left(\frac{2\pi}{\Lambda}x_6\right)\right]. \tag{11}$$

Eq. (11) shows explicitly that the detected power is a function of the horizontal spatial coordinate x_6, it is independent of y_6 and is proportional to the local vertical height of the grating under test. The power depends also on r_6 and on the period of the grating Λ. The vertical amplitude profiles are obtained by scanning a small region of the grating.

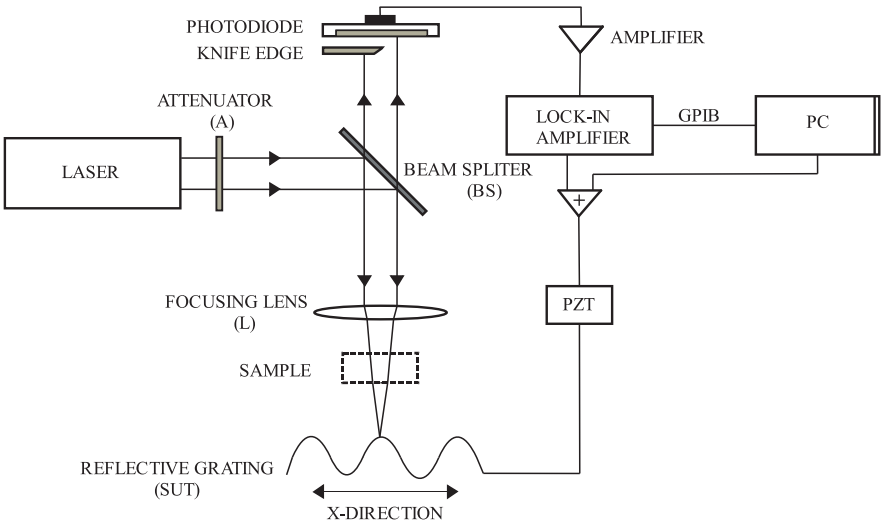

Fig. 4. Homodyne KED profilometer for measuring r_6.

Initially the system is adjusted to the best focusing conditions for zero concentration ($r_6 = 1\ \mu m$). Under this condition, increasing c will increase r_6 and this in turn will cause a decrease of the vertical amplitude recorded according to Eq. (11). Fig. 5 shows plots for a decrease in 75 and 50% of the vertical amplitude normalized with respect to best focused. The respective values of r_6 are 1.08 and 1.19 μm for the 600 l/mm grating and 1.47 and 1.81 μm for 300 l/mm, respectively.

These results demonstrate that the sensitivity of the system can properly be adjusted by only selecting the grating pitch. In the next section we give experimental results.

3. Experimental results

To illustrate our proposal the system was tuned at two different sensitivities for concentrations below 10%,

a) For glucose concentrations from 0 to 1.25 g/dl in steps of 0.25 g/dl. In this case a grating of 600 l/mm was used.
b) For concentrations between 1.5 and 7.5 g/dl in steps of 1.5 g/dl, a grating of 300 l/mm was used.

For each grating the experimental process was as follows. The system was adjusted to obtain the best focusing conditions with the sample of zero concentration and then a region of the grating was scanned and recorded. After that, a known amount of glucose was poured into the container and the mixture was left to settle. Then, the same region of the grating was scanned again. The process was repeated for each new glucose concentration. The repeatability of the measurements was verified by scanning several times the same region. In each scan 200 pixels were recorded. Instead of determining the concentration using only one local height of the grating, higher accuracy is obtained calculating the rms of the overall height distributions. The solution was prepared with clinical glucose patron commercially available and care was taken to assure that the transmittance of the sample remained constant. All the measurements were made at constant temperature of 25 °C. Every measurement took approximately 1 min. Fig. 6 shows plots of the normalized vertical amplitudes for different glucose concentrations. Fig. 6a) is for concentrations in the range between 0 and 1.25 g/dl in steps of 0.25 g/dl. Fig. 6b) is for concentrations in the range between zero and 7.5 g/dl in steps of 1.5 g/dl. In both figures smaller amplitudes correspond to higher concentrations.

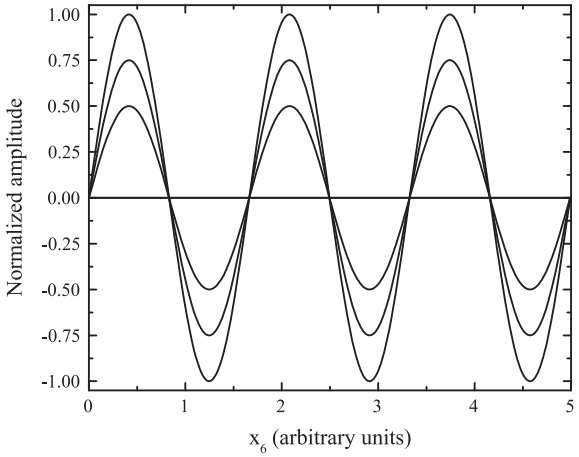

Fig. 5. Decrease of the vertical amplitudes as a function of defocus as described in the text.

As it can be noticed from Fig. 6, as the glucose concentration increases the vertical amplitude decreases in agreement with Eq. (11). We want to remark that the homodyne KED can detect subsurface features and were filtered out as in our calculations are not required. Fig. 7 shows plots of the rms values that correspond to the measurements depicted in Fig. 6.

With the above results we estimate that the minimum step of glucose concentration that can be detected with the grating of 600 l/mm is approximately 0.06 g/dl and 0.25 g/dl for the 300 l/mm grating. By using a laser with a shorter wavelength will allow using gratings with higher spatial frequencies giving the possibility of recording lower values of concentrations.

With the results obtained with the two gratings we get an overall plot of r_6 as a function of c, which as mentioned resides in a vicinity around regions I and II. The plot is shown in Fig. 8. The corresponding fitted curve is included.

The fitted equation obtained is given as,

$$r_6(c) = 1.051 \times 10^{-6} + 1.024 \times 10^{-7}\, c, \tag{12}$$

where c is measured in g/dl and r_6 is measured in meters. This equation is in agreement with the one predicted theoretically in Eq. (7) and its plot is shown in Fig. 8.

A1

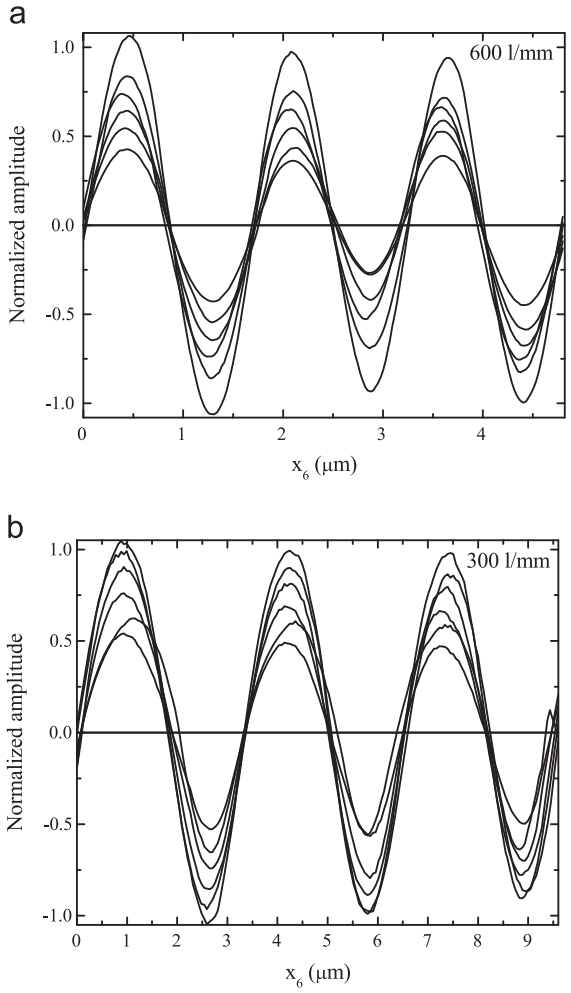

Fig. 6. Experimental normalized vertical amplitude for the two gratings (a) 600 and (b) 300 lines/mm. The corresponding concentrations are described in the text.

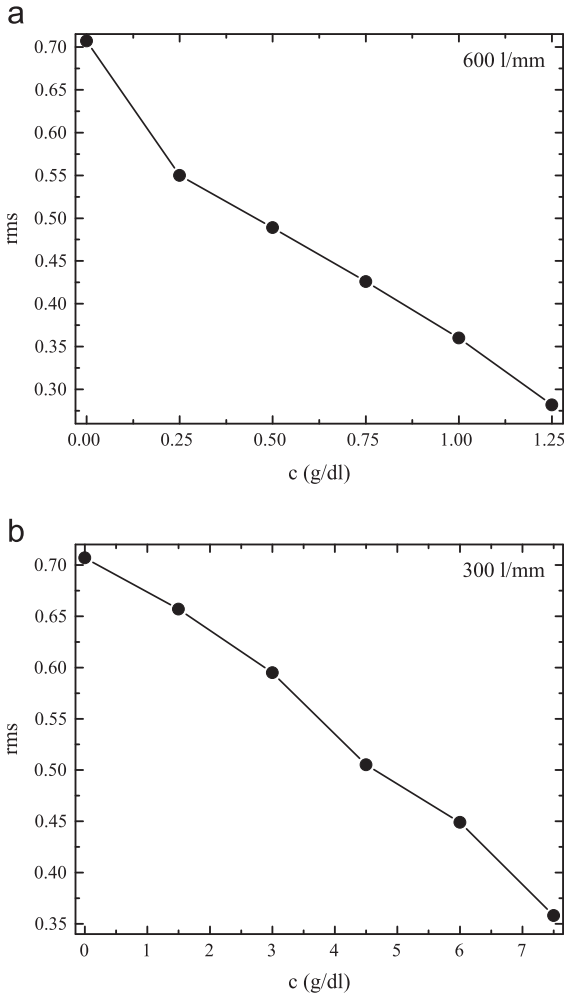

Fig. 7. Plots of the rms for the normalized vertical heights corresponding to Fig. 6 for (a) 600 and (b) 300 lines/mm pitches as a function of glucose concentration.

Substituting Eq. (12) in (6) we obtain,

$$n_S(c) = 1.3312 + 41.841(0.051 \times 10^{-6} + 1.024 \times 10^{-7}\, c)^{0.5881}, \tag{13}$$

Eq. (13) shows that for small values of concentration a linear relation is obtained as a function of the refractive index as was predicted in our theoretical description.

The plot in Fig. 9, obtained with Eq. (13), shows the overall behavior of n_S as a function of c. The plot resides in region I and extends slightly into region II. It is important to notice how the pitches of the gratings were tuned to construct each particular region of the overall plot. The system can be tuned to other regions by using gratings with other pitches.

4. Conclusions

We have applied defocusing properties of Gaussian beams to measure the refractive index as a function of the concentration in thin transparent samples. We first calculated theoretically the propagation of the beam across the system to find an equation that relates the refractive index as a function of defocus. With this general equation we constructed the theoretical basis and found three regions that describe the overall shape of the corresponding plot between them in any range. As the method is based on measuring accurately the defocus caused by variations in the sample concentration we took advantage of the homodyne knife edge detector while profiling a calibrated reflective grating. Our proposal may be useful to avoid or alleviate discrepancies found in the literature of curves reported for different substances, especially for glucose. Our theory is limited to substances whose refractive index increases with concentration.

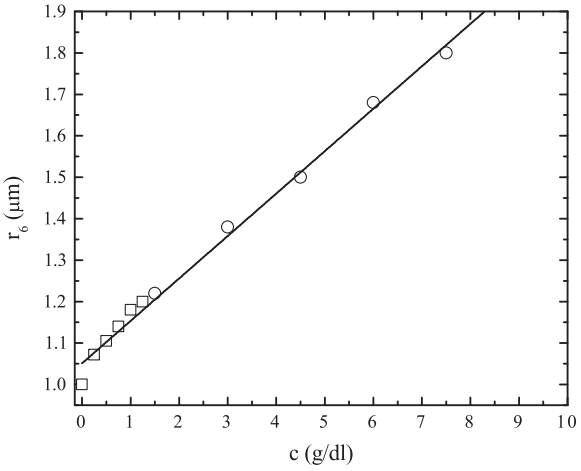

Fig. 8. Experimentally obtained r_6 as a function of c. The region with squares was obtained with the 600 l/mm grating and the circled with the 300 l/mm. The solid line corresponds to the fitted equation.

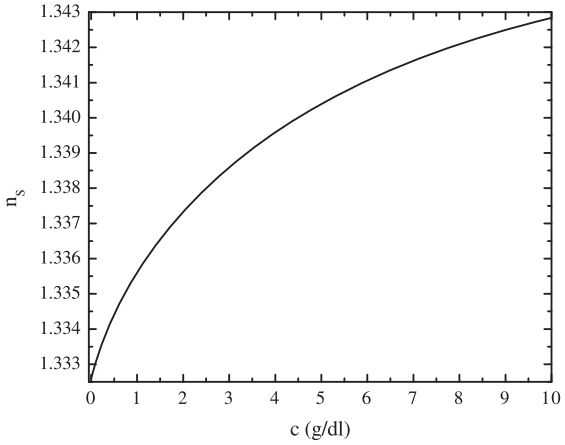

Fig. 9. n_s as a function of c, obtained with Eq. (13) for λ=632.8 nm.

Acknowledgments

We thank CONACyT for partial support.

References

[1] Y.L. Yeh, Optics and Lasers in Engineering 46 (2008) 666.
[2] R.C. Weast, CRC Handbook of Chemistry and Physics, 61st, CRCPress, Inc, Boca Raton, FL, 1980.
[3] Kirill V. Larin, Taner Akkin, Rinat O. Esenaliev, Massoud Motamedi, Thomas E. Milner, Applied Optics 43 (2004) 3408.
[4] Y. Liu, P. Hering, M.O. Scully, Applied Physics B 54 (1992) 18.
[5] W. Mahmood bin Mat, Yunus, Azizan bin Abdul Rahman, Applied Optics 27 (1988) 3341.
[6] Chien-Chang Chiao-Ling Wong, Wei-Bin Huang, Wen-Ming Lu, Jo-Shu Chen, Biochemical Engineering Journal 69 (2012) 32.
[7] T.W. Yang, Z.M. Rao, X. Zhang, Q. Lin, H.F. Xia, Z.H. Xu, S.T. Yang, Journal of Basic Microbiology 51 (2011) 650.
[8] J.Y. Lee, S.K. Tsai, Optics Communication 284 (2011) 925.
[9] K. Chen, C. Hsu, D.-C. Su, Applied Optics 42 (2003) 5774.
[10] M. Chiu, S. Wand, R. Chang, Optics Letters 30 (2005) 233.
[11] K.H. Chen, J.-H. Chen, S.-W. Kuo, T.-T. Kuo, M.-H. Lai, Optics Communication 283 (2010) 2812.
[12] C. Wang, M. Kaya, C. Wang, Journal of Biomedial Optics 17 (3) (2012).
[13] T.Q. Lin, Y.L. Lu, C.C. Hsu, Optics Express 26 (2010) 27560.
[14] M. Cywiak, J. Murakowski, G. Wade, International Journal of Imaging Systems and Technology 11 (2000) 164.
[15] J. Murakowski, M. Cywiak, B Rosner, D. van der Weide, Optics Communication 185 (2000) 295.

Optics Communications 331 (2014) 239–243

Contents lists available at ScienceDirect

Optics Communications

journal homepage: www.elsevier.com/locate/optcom

Measurement of glucose concentration in a thin turbid medium by a transmitted Gaussian beam

Joel Cervantes-L [a], Moisés Cywiak [a,*], Octavio Olvera-R [a], David Cywiak [b]

[a] Centro de Investigación en Óptica A.C., León, Guanajuato, Leon 37150, Mexico
[b] Centro Nacional de Metrología (CENAM), El Marqués, Querétaro, Santiago de Querétaro 76246, Mexico

ARTICLE INFO

Article history:
Received 10 March 2014
Received in revised form
10 May 2014
Accepted 4 June 2014
Available online 26 June 2014

Keywords:
Glucose concentration
Gaussian beams
Homodyne detection
Turbid medium
Intralipid™
Scattering medium

ABSTRACT

We show that it is possible to measure glucose concentration in a thin sample containing a turbid medium that simulates optical properties of biological tissue by recording the profile of a sinusoidal reflective grating by means of a laser Gaussian beam. We have described a similar approach for the case of transparent samples in a previous report. Although due to the turbidity of the sample the laser beam is scattered, we show that the probe beam is still sensitive enough to allow the detection of the grating profile. We describe how the changes recorded by the system, when profiling a region of the grating, allow us to determine the concentration of glucose in the turbid medium. We include experimental results.

1. Introduction

Measurement of glucose concentration in thin turbid media representing optical scattering properties of biological tissue is of major importance. These samples are typically prepared by means of phantoms containing intralipid or nanospheres [1–5]. Techniques to determine glucose concentration in these samples can be classified mainly in two: by transmitted and/or reflected light. When reflective light is used, the techniques are mainly of the type of optical coherence tomography (OCT), refractometric methods and Raman spectroscopy polarization [6–10]. These techniques generally exhibit low sensitivity (signal-to-noise-ratio) thus, requiring high glucose concentrations [8], resulting in imprecise values that require statistical algorithms to improve the estimation of the measurements. In contrast, techniques that use transmitted light are mainly based on the photo-acoustic effect (PA) [9,11–16]. However, the PA signal can vary between measurements, meaning that differences of PA signal can be affected by other factors such as physiological change, temperature and mechanical stability of the sample [13].

In [17] we have described an optical technique for measuring glucose concentration in thin transparent samples. In this report we extend the referred optical technique to measure glucose concentration in a turbid medium that simulates optical scattering properties of biological tissue.

Phantoms made of 1% intralipid solution are commonly used for experiments that simulate optical scattering properties of biological tissue [18–20]. Our sample has a higher concentration (2.5%) to demonstrate the usefulness of our pure optical technique; this concentration gives optical properties that fall within the range of human breast and skin tissue [21,22]. The maximum width of our sample may be up to 5 mm. Our technique consists in profiling a calibrated reflective grating using a Gaussian probe beam transmitted through the turbid sample. In the next sections we describe our proposal and give our experimental results.

2. Analytical description

Fig. 1 depicts the experimental setup which is based on the homodyne knife-edge detector (KED) [23,24] as done in our previous report for transparent samples [17]. For convenience we briefly describe KED.

The illuminating source is a non-polarized He–Ne laser beam ($\lambda = 632$ nm). The laser beam is directed towards a beam splitter (BS). The beam reflected by BS is transmitted through a focusing lens (L) and directed towards the surface of the grating through the turbid sample (S). The reflective grating is a commercially available holographic grating with a sinusoidal profile. The beam reflected by the grating propagates again through the sample and

* Corresponding author.
E-mail address: moi@cio.mx (M. Cywiak).

http://dx.doi.org/10.1016/j.optcom.2014.06.025
0030-4018/

A2

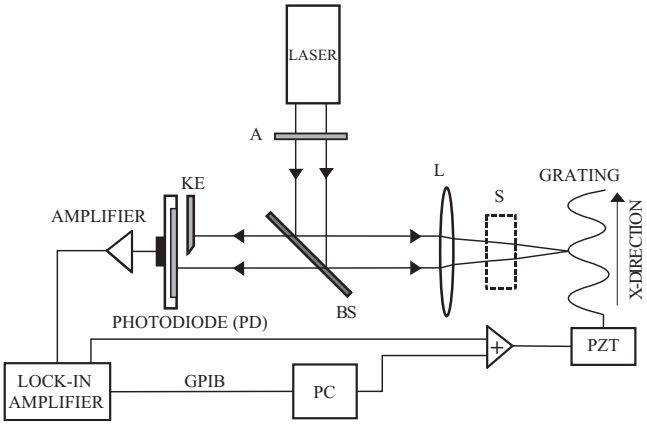

Fig. 1. Experimental setup of the KED.

through the focusing lens and is directed to a photodiode (PD) partially blocked by a knife-edge (KE). The turbid sample is in a glass container with dimensions 5.0 × 5.0 × 5.0 mm. An attenuator (A) limits the incident power light at the surface under test to avoid damaging of the grating surface due to excessive heating. The focusing lens is a 100× objective microscope, with 1 cm working-distance to allow the placement of the sample. Initially, the lens and the grating are adjusted to focus the Gaussian beam when the sample is a liquid transparent medium as described in [17]. When the transparent sample is replaced by the turbid one, the transmitted light is scattered; we show below that the lens is still useful under this condition, allowing us to detect the grating profile.

In [23,24] it is shown that, when the sample is not placed in the optical path, or equivalently, when the sample is a virtual one with refractive index equal to one the power collected by the photodiode is given by,

$$P_{out}(x_0,y_0) = -i\frac{8\,P_0}{\lambda\, r_0^2}\delta_0 \int_{-\infty}^{\infty}\int_{-\infty}^{\infty} \exp\left(-2\frac{(x-x_0)^2+(y-y_0)^2}{r_0^2}\right) \times erf\left(i\frac{x-x_0}{r_0}\right)\frac{\partial}{\partial x}h(x,y)dxdy, \quad (1)$$

where $h(x,y)$ represents the surface profile of the grating considered in a plane (x,y), P_0 is the beam power which is constant. The semi-width of the Gaussian probe beam is represented by r_0 and focused at (x_0,y_0), λ is the wavelength of the illuminating source. In Eq. (1) the partial derivative of the height distribution appears as a consequence of a first order expansion due to the vibration of the grating, with small amplitude δ_0 as described in [23,24]. $erf(\,)$ is the error function and $i=\sqrt{-1}$. It is possible to calculate the double integral in Eq. (1) in a closed form, taking into account that $h(x,y)$ represents a one-dimensional sinusoidal function with period Λ, we obtain,

$$P_{out}(x_0,y_0) = \frac{8\pi^2\delta_0}{\lambda\Lambda}P_0\exp\left(-\frac{\pi^2 r_0^2}{2\Lambda^2}\right)erf\left(\frac{\pi\, r_0}{\sqrt{2}\Lambda}\right)\left[h_0\ \sin\left(\frac{2\pi}{\Lambda}x_0\right)\right]. \quad (2)$$

Eq. (2) demonstrates that the power collected by the photodiode is proportional to the local vertical height of the grating, the term in square brackets. Thus, in order to record the vertical profile over a determined region, it is necessary to perform a linear scan.

A plot of Eq. (2) for the two different gratings used in our experiments, 600 and 300 lines/mm is depicted in Fig. 2 for a constant local vertical height.

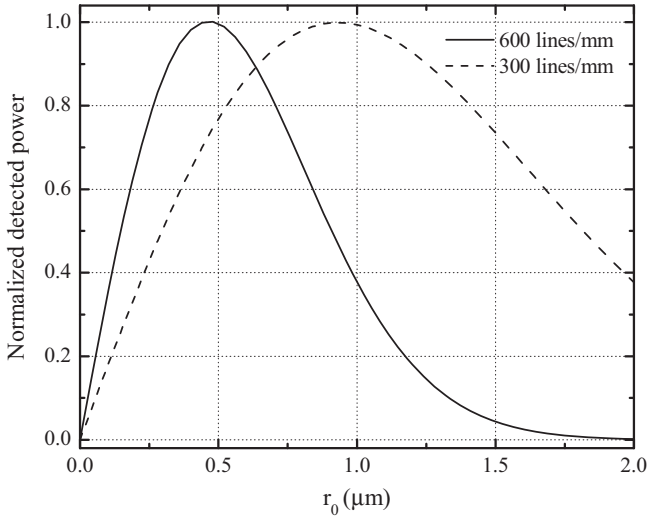

Fig. 2. Normalized detected power as a function of r_0 according to Eq. (2) for gratings 600 and 300 lines/mm.

It can be noticed from Fig. 2 that for both gratings the amplitude of the detected power decreases for $r_0 > 1$ μm. In our experiments larger semi-widths are attained.

Eq. (2) is the key of our proposal; however, before describing how it is applied to determine glucose concentration in turbid media, it will be useful to refer to our previous report [17] for measuring glucose concentration in thin transparent samples. In the referred report it is described that a linear relation between the semi-width and the concentration is expected for low concentration values, as the beam is well focused, and the surface under test is in the Rayleigh region where small changes result linear. Experimentally, it was shown in the reference, that for a thin transparent sample (< 5 mm) increasing glucose concentration (c) of the sample results in a linear increase of r_0; this linear relation holds well in a range up to 10 g/dl. It should be noticed however, that a linear function between r_0 and c, does not imply a linear relationship between the detected power and c as stated by Eq. (2). When a turbid media substitutes the transparent media, as it will be seen below, a linear relationship is found, contrary to the transparent case.

The measuring procedure is as follows. First, the system is adjusted to best focusing conditions with a sample with zero glucose concentration (smallest r_0 value). Then, a scan of a region of the grating is recorded. Next, the same region of the grating is recorded for different glucose concentrations. As indicated, increasing c in the sample results in a linear increase of r_0; thus, due to the exponential term in Eq. (2) the heights of the vertical profiles recorded will decrease. This effect can be appreciated in the plot of Fig. 2.

Eq. (2) further shows that the collected power is also a function of the period of the grating Λ.

Its effect can be visualized in the following way. The system is first adjusted to a minimum r_0 for $c=0$. Then, as indicated, as in our case $r_0 > 1$ μm, the recorded profiles will exhibit maximum height; increasing c will result in reducing the vertical heights of the recorded profiles. Let us now consider two particular cases of reducing the vertical profiles to 75 and 50% with respect to the case $c=0$. The 600 lines/mm grating will require defocusing values of 1.08 and 1.19 μm respectively; these values correspond to samples with concentrations of 0.3 and 0.9 g/dl respectively. In contrast the grating of 300 lines/mm will require higher defocusing, 1.47 and 1.81 μm, corresponding to higher concentrations 4.5 and 7.5 g/dl [17]. Table 1 summarizes these results.

Table 1
Experimental glucose concentrations and defocusing required for diminishing in 75 and 50% of the maximum amplitude for both gratings: 600 and 300 lines/mm, for a thin transparent sample as reported in [17].

Decreasing amplitude (%)	Glucose concentration c (g/dl) $\Lambda_{600}/\Lambda_{300}$	Semi-width r_0 (μm) $\Lambda_{600}/\Lambda_{300}$
75	0.3/4.5	1.08/1.47
50	0.9/7.5	1.19/1.81

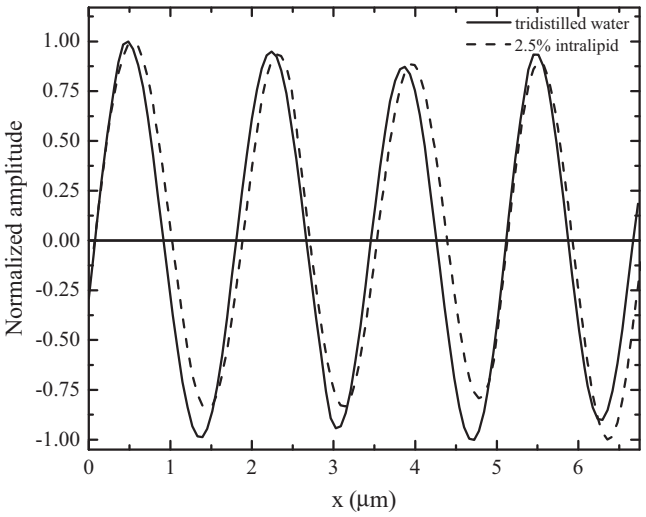

Fig. 3. Normalized grating profiles recorded with the KED for the turbid and transparent samples on the conditions described in the text.

It has to be remarked that the data in Table 1 is valid only for a thin transparent sample as described in [17]. The purpose of this table is illustrating how Λ permits tuning the sensitivity of the system to a desired range of glucose concentration. Namely, to determine low concentrations, a high pitch grating is necessary. In contrast for measuring high concentrations a grating with a low pitch is used.

It can be noticed that the detected power is not a linear function of c, in contrast to the linear relation of r_0 vs. c. We remark that the data in Table 1 is valid only for the case of a transparent sample. It will be seen below, that for a turbid media, due to scattering r_0 results much larger causing also a linear relationship between c and the detected power.

Now, when the turbid sample is placed in the optical path as depicted in Fig. 1, scattering of the beam occurs. In Fig. 3, we show the normalized experimental profile recorded when the turbid sample is placed in the optical path. For comparative purposes, Fig. 3 also includes a normalized plot of the profile obtained when the sample consists of pure transparent water with the same width. For recording the profile when the turbid sample is placed in the setup, it was necessary to increase the illuminating power of the laser by 5 times (adjusting the attenuator) and also to increase the gain of the amplifier 25 times as compared with the conditions used with the transparent sample.

Fig. 3 demonstrates experimentally that for the thin turbid sample it is possible to record the profile of the reflective grating with reasonable accuracy. We conclude that appropriate conditions remain for profiling the grating in the presence of the turbid sample.

To proceed further, we must demonstrate that the system is sensitive to glucose concentration independently of the inherent optical parameters of the turbid medium. For this purpose we took different concentrations of intralipid up to 2.5% in steps of 0.5%. With this set of intralipid concentrations we performed the procedure described above for different glucose concentrations. We found the same linear relation between the *rms* of the recorded vertical profiles as a function of c for all the cases exactly as in the case of the transparent sample. This result shows that the system is sensitive to changes in glucose concentration independently of the optical properties of the turbid sample.

Table 2
Set of used intralipid concentrations and their corresponding optical parameters estimated from [21,22,25].

Intralipid concentration (%)	Scattering coefficient μ_s (cm^{-1})	Reduced scattering coefficient μ_s' (cm^{-1})	Anisotropy coefficient g	Absorption coefficient μ_A (cm^{-1})
0.5	5.0	1.0	0.8	0.6
1.0	12.0	2.5	0.8	0.6
1.5	20.0	4.0	0.8	0.7
2.0	30.0	6.0	0.8	0.7
2.5	40.0	8.0	0.8	0.75

Approximate values of the optical parameters of the phantoms used in our experiments are given in Table 2.

In the next section we give experimental results for glucose determination.

3. Experimental results

In this section we describe the results for the maximum concentration conducted in our experiments which consisted of a 2.5% intralipid prepared from a 20% stock solution commercially available. Its estimated optical parameters are given in Table 2. Known amounts of glucose were added to the solutions as described below.

The system was tuned at two sensitivities in the following way: For glucose concentrations less than 1 g/dl we used a grating of 600 lines/mm. For concentrations greater than 1.5 g/dl we used a grating of 300 lines/mm.

The experimental procedure was as follows. First, the sample of 2.5% intralipid with zero glucose concentration was placed in the optical path between the focusing lens and the grating as depicted in Fig. 1. Its absolute position is irrelevant as shown in [17]. The grating position was adjusted until a maximum vertical height profile was obtained. This adjustment corresponds to zero glucose concentration and best focusing conditions. This profile is taken as a reference value and normalized.

Next, to obtain a relation of c as a function of the recorded vertical heights, known amounts of c were added to the intralipid sample. Care was taken in maintaining the same intralipid concentration. Then, the same region of the grating was scanned again. The process was repeated for each new glucose concentration. Additionally the sensitivity of the system was selected by replacing the pitch of the grating as described above. The measurements were made at constant temperature of 25 °C.

Fig. 4 shows plots of the reflection profile of the gratings recorded by the system for different glucose concentrations, where the plot of zero glucose concentration has been normalized. Fig. 4a is for concentrations in the range between 0.0 and 1.0 g/dl in steps of 0.25 g/dl. Fig. 4b is for concentrations in the range between 0.0 and 7.5 g/dl in steps of 1.5 g/dl. In both figures the amplitude of the profiles decreases with concentration.

Fig. 4 indicates that steps of 0.25 g/dl can easily be distinguished with the grating of 600 lines/mm and steps of 1.5 g/dl with the 300 lines/mm. The resolution can be highly improved by calculating the *rms* values of the overall profiles instead of using the local vertical heights.

A2

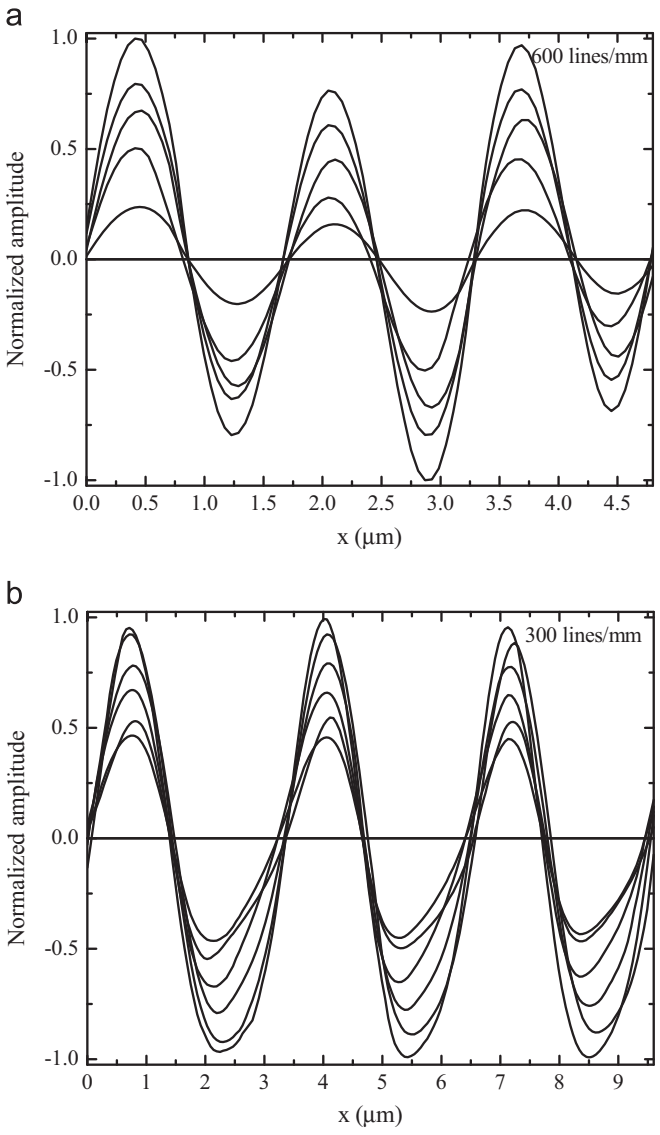

Fig. 4. Experimental normalized vertical amplitudes for the two gratings for different glucose concentrations. (a) Profiles of the 600 lines/mm grating for concentrations between 0.0 and 1.0 g/dl in steps of 0.25 g/dl. The highest profile corresponds to 0.0 g/dl. The lowest profile corresponds to 1.0 g/dl. (b) Profiles for the 300 lines/mm grating for concentrations between 0.0 and 7.5 g/dl in steps of 1.5 g/dl. The highest profile corresponds to 0.0 g/dl. The lowest profile corresponds to 7.5 g/dl.

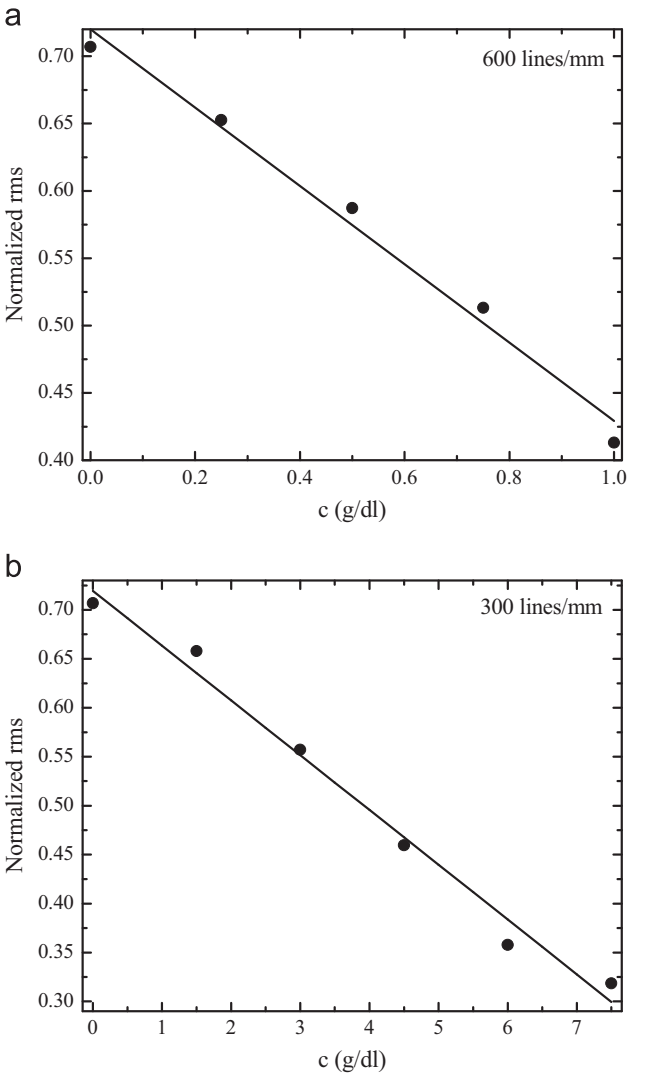

Fig. 5. Experimental normalized *rms* as a function of *c*. (a) obtained with the 600 lines/mm grating and (b) 300 lines/mm. The continuous lines correspond to the fitted equations.

Fig. 5 shows plots of the experimental *rms* values of the recorded vertical heights as a function of *c*. The solid lines represent the fitted linear curves given by Eqs. (3-a) and (3-b) given below.

The fitted linear equations are given as,

$$rms_{600} = -0.2910c + 0.7214, \quad (3-a)$$

$$rms_{300} = -0.0559c + 0.7195, \quad (3-b)$$

where rms_{600} and rms_{300} are the *rms* values of the profiles for 600 lines/mm and 300 lines/mm gratings correspondingly and *c* is given in g/dl.

According to Table 1 a non-linear response between the detected power and *c* is obtained for the transparent medium in contrast to the case of the turbid medium as stated by Eqs. (3-a), (3-b). This is due to scattering which highly widens the beam. Thus, changes in *c* will induce very small relative changes in r_0 compared with the transparent case. Graphically, this corresponds to a very small region of the plot of Fig. 2 around a large value of r_0 giving a linear response. Although the signal is very small, as it can be seen in Fig. 3, KED has a very high sensitivity making it appropriate to perform the detection of glucose concentration.

To further increase the sensitivity to lower concentrations, gratings with higher spatial frequencies can be used; this in turn will require using a laser with a shorter wavelength. However, the scattering coefficient increases slightly and this has to be considered.

To test our system with a real biological sample, we conducted the following experiment: a small portion of chicken skin taken from a leg without any preparation was held by its peripheral edge and left to dry naturally for several hours. The geometrical thickness was approximately 1 mm. The sample was placed in the optical path of the system as depicted in Fig. 1. A plot of the grating recorded through the skin-sample is shown in Fig. 6. Additionally, for comparative purposes the same region of the grating is also plotted for different concentrations of intralipid. In order to have a one-to-one comparison, we set the attenuator to appropriate conditions to get approximately the same vertical heights. Some undesirable features on the profile obtained with the chicken skin due to the highly scattered beam can be appreciated and are irrelevant as can be filtered out of the profile.

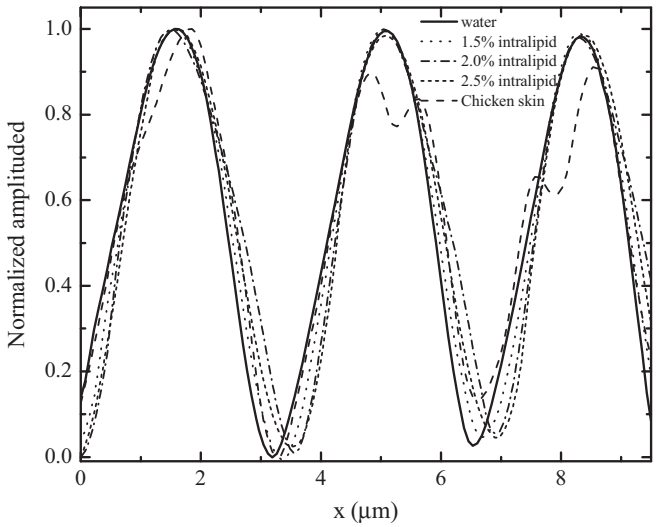

Fig. 6. Comparison of the grating profile recorded with the KED for a chicken skin-sample compared with samples of pure water and intralipid with concentrations of 1.5, 2.0 and 2.5%. The gain of the amplifier and the attenuator were adjusted to attain approximately the same vertical heights.

Fig. 6 clearly shows that it is still possible to recover the grating profile, making apparent the usefulness of our technique when using real biological samples. Although we do not have precise information of the optical parameters of the chicken skin, based in [26], the parameters are within the following ranges: $10.85 < \mu_s' < 21.42\ \mathrm{cm}^{-1}$, $0.16 < \mu_a < 0.59\ \mathrm{cm}^{-1}$ and $0.7 < g < 0.9$. The experiment was carried out using the 300 lines/mm grating. It was not possible to obtain the profile with the 600 lines/mm grating with the power available from our laser which is 3 mW.

Finally, we found experimentally that for a 5 mm sample width, a concentration of 3% of intralipid is the upper limit that allows us detecting the grating. Using higher power and/or infrared light should enhance the penetration depth.

It is important to remark that our proposal requires calibrating the system with a sample of zero glucose concentration before performing the measurements. This limitation can possibly be overcome taking advantage that the system has a linear response as a function of glucose concentration, being independent of the scattering and absorption properties of the medium. Thus, if a relationship of the optical properties between different media could be obtained by other means, it would be sufficient to calibrate only one medium; future research in this direction is necessary, taking into account the length of the turbid media.

Before finishing this report we provide a brief comparison of our technique with other methods: first, from Fig. 5 we can notice that for the 600 lines/mm grating a change of 0.5 g/dl results in a change of approximately 15% in the detected signal. For the 300 lines/mm grating, used for high concentration measurements, the same glucose change results in a change of approximately 3%. For comparison, in the polarization state of backscattered laser light technique [11] the corresponding signal change is 2% and for an OCT technique [6] is 4%. Furthermore, it should be noticed that the mentioned techniques cannot be tuned to a region of interest as is the case of our technique.

4. Conclusions

We have shown that it is possible to record the profile of a sinusoidal reflective grating by means of a laser Gaussian beam that has been transmitted through a thin sample that contains a turbid medium of an intralipid solution. This solution simulates optical properties of biological tissue. An analytical expression relating the vertical height profile of the reflective grating measured by the system as a function of glucose concentration in the turbid medium was obtained. In this way it is possible to calibrate the system to determine glucose concentration in thin turbid media with high repeatability. To show the performance of our technique using real biological samples, we performed measurements with a sample of chicken skin taken from a leg without any preparation. The system was capable of recording the grating profile for this sample with reasonable accuracy, making apparent the usefulness of our technique for real biological samples.

References

[1] M.L. Dong, K.G. Goyal, B.W. Worth, S.S. Makkar, W.R. Calhourn, L.M. Bali, S. Bali, J. Biomed. Opt. 18 (2013) 087003.
[2] Q. Ye, et al., J. Biomed. Opt. 16 (9) (2011) 097001.
[3] P. Di Ninni, F. Martelli, G. Zaccanti, Phys. Med. Biol. 56 (2) (2011) N21.
[4] R. Michels, F. Foschum, A. Kienle, Opt. Express 16 (8) (2008) 5907.
[5] H. Ding, J.Q. Lu, K.M. Jacobs, X.H. Hu, J. Opt. Soc. Am. A 22 (2005) 1151.
[6] M. Kirillin, A. Priezzhev, M. Kinnunen, E. Alarousu, Z. Zhao, J. Hast, R. Myllylä, A. Priezzhev, G. Cote, Proc. SPIE 5325 (2004) 164–174.
[7] K.V. Larin, T.V. Ashitkov, I. Larina, I. Petrova, M. Eledrisi, M. Motamedi, R.O. Esenaliev, Proc. SPIE (2004) 285–290 (0277-786 × 5474).
[8] K. Larin, I. Larina, M. Motamedi, V. Gelikonov, R. Kuranov, R. Esenaliev, Proc. SPIE Int. Soc. Opt. Eng. 4263 (2001) 83.
[9] Erkki Alarousu, Jukka Hast, Matti Kinnunen, Mikhail Kirillin, Risto Myllyla, Jerzy Plucinski, Alexey Popov, Alexander Priezzhev, Tuukka Prykari, Juha Saarela, Zuomin Zhao, Proc. SPIE (2004) (5474-05).
[10] A.A. Zanishevskaya, A.V. Malinin, Yu.S. Skibina, V.V. Tuchin, M.V. Chainikov, V.I. Beloglazov, I.Yu. Silokhin, A.M. Ermakova, Opt. Spektrosk. 115 (2) (2013) 266.
[11] G.A. Kafidova, E.T. Aksenov, V.M. Petrov, Proc. SPIE 8803 (2013) 880306.
[12] Daniel Côté, I. Alex Vitkin, Opt. Express 13 (2005) 148.
[13] Z. Zaho, Pulsed photoacoustic techniques and glucose determination in human blood in tissue, Ph.D. thesis (University of Oulu, 2002).
[14] J. Kottmann, J.M. Rey, J. Luginbühl, E. Reichmann, M.W. Sigrist, Biomed. Opt. Express 3 (4) (2012) 667.
[15] K. Larin, A. Oraevsky, Proc. SPIE 3726 (1998) (576-563).
[16] Raju Poddar, Joseph Tomas Andrews, Pratyoosh Shukla, Pratima Sen, Medical Physics, Instrumentation and Detectors (2008), ⟨arXiv:0810.5755v1⟩ [physics. med-ph].
[17] Joel Cervantes-L, Moisés Cywiak, Octavio Olvera-R, Arquímedes Morales, Opt. Commun. 309 (2013) 108–113.
[18] K. Jakobsohn, M. Motiei, M. Sinvani, R. Popovtzer, Int. J. Nanomed. 7 (2012) (4707–471).
[19] Canpolat, M. Optik (Munich, Ger.) 122 (2011) 887–890.
[20] J.S. Dam, C.B. Pedersn, T. Dalgaard, P.A. Fabricius, P. Aruna, S Anderson Engles, Appl. Opt. 40 (7) (2001) 1155.
[21] Homa Assadi, Rafii Karshafian, Alexandre Douplik, Int. J. Photoenergy Novel Photomed. Issue (2014).
[22] J.L. Sandell, T.C. Zhu, J. Biophotonics 4 (2011) 773.
[23] M. Cywiak, J. Murakowski, G. Wade, Int. J. Imaging Syst. Technol. 11 (2000) 164.
[24] J. Murakowski, M. Cywiak, B. Rosner, D. van der Weide, Opt. Commun. 185 (2000) 295–303.
[25] B. Aernouts, E. Zamora-Rojas, R. Van Beers, R. Watté, L. Wang, M. Tsuta, W. Saeys, Opt. Express 21 (26) (2013) 32450.
[26] A. Singh, A.E. Karsten, J.S. Dam, Proc. Int. Conf. World Assoc. Laser Ther. (2008) 165–169.

Refractive index and geometrical thickness measurement of a transparent pellicle in air by Gaussian beam defocusing

Octavio Olvera-R, Moisés Cywiak,* Joel Cervantes-L, and Arquímedes Morales

Centro de Investigaciones en Óptica A. C. León Gto., Mexico

*Corresponding author: moi@cio.mx

Received 22 January 2014; accepted 18 February 2014;
posted 4 March 2014 (Doc. ID 205260); published 2 April 2014

We demonstrate that it is possible to measure the local geometrical thickness and the refractive index of a transparent pellicle in air by combining the diffractive properties of a Gaussian beam with the analytical equations of the light that propagates through a thin layer. We show that our measurement technique is immune to inherent piston-like vibrations present in the pellicle. As our measurements are based on characterizing properly the Gaussian beam in a plane of detection, a homodyne technique for this purpose is devised and described. The feasibility of our proposal is confirmed by measuring local geometrical thicknesses and the refractive index of a commercially available stretch film.

OCIS codes: (070.0070) Fourier optics and signal processing; (070.7345) Wave propagation; (120.0120) Instrumentation, measurement, and metrology; (120.3940) Metrology; (310.0310) Thin films; (310.6860) Thin films, optical properties.

http://dx.doi.org/10.1364/AO.53.002267

1. Introduction

Measuring locally the geometrical thickness and the refractive index of transparent pellicles in air (which are commercially available in thicknesses from 2 to 200 μm) represents a difficult task because of an inherent and incessant vibration present on the pellicle. At first impression, one may think that interferometric techniques, which lead to nanometric resolutions on films, deposited on some kind of substrate [1–5] could be used. However, when the pellicle is set in air and supported at its peripheral edge, its center undergoes a piston-like continuous vibration even in a controlled ambient. Thus interferometric techniques cannot be used, as the fringe pattern will constantly vibrate, resulting in erroneous measurements.

An approach that avoids using interferometric techniques to alleviate the problem mentioned above can be found in [6]. The sample under test is placed between two polarizers. Light is directed to the pellicle through one of the polarizers while it is tilted at different angles to be analyzed by the light that is transmitted through a second polarizer or analyzer. The angle that subtends the pellicle with the optical axis is the main parameter of the technique and has to be calculated with high accuracy. The refractive index and thickness of the sample are obtained by mathematical relations based on measuring at some specific angles. However, in the mentioned report the problem of the random and incessant pellicle vibrations that induce variations on the angle is not considered. These vibrations in turn, depending on the distance of measurement, may introduce severe variations in the readings.

In this work, we propose an alternative approach that allows measuring locally the refractive index and geometrical thickness of a pellicle in air. As

1559-128X/14/112267-06$15.00/0

shown below, our proposal results are basically immune to the inherent vibrations of the pellicle. The technique is based on the diffractive properties of Gaussian beams. We demonstrate that the sample can be placed in the path of a focusing beam where movements of the pellicle do not affect the semi-width of the beam at a plane of detection. We combine the diffractive properties of Gaussian beams with the analytical equations of the transmitted light by a pellicle in air. As our technique requires measuring the semi-width of the diffracted Gaussian beam with high accuracy, we devised a homodyne technique to improve the accuracy of our proposal. In the next sections, we describe our analytical proposal and give experimental results.

2. Analytical Description

In Fig. 1, a He–Ne laser beam is directed to a focusing lens placed on a coordinate plane (x_1, y_1) at a distance z_0 from the laser output. The lens is considered very thin and large enough to allow focusing the incoming Gaussian beam without any visible truncation. Let z_T be the distance from the (x_1, y_1) plane up to a plane of observation with coordinates (ξ, η). As depicted, the pellicle under test (the dashed rectangle in the drawing) is placed transversal to the optical axis z. Let t be the geometrical thickness of the sample that is exaggerated in the figure for descriptive purposes; thus,

$$z_T = z_1 + t + z_2, \tag{1}$$

where z_1 and z_2 are the distances depicted in Fig. 1 that can be chosen arbitrarily, as it will be demonstrated below.

The overall propagation of the Gaussian beam through the system can be calculated by means of the Fresnel diffraction integral [7]. For this, the laser beam is characterized by means of its semi-width and its divergence.

Let us consider a virtual pellicle, that is, a pellicle with geometrical thickness t and refractive index equal to one. For this condition we calculate the overall propagation from the laser up to the plane of observation, and we plot the semi-width of the Gaussian beam as a function of distance z_T. These calculations allow us to characterize all the parameters involved in the propagation of the beam and are adjusted with those obtained experimentally.

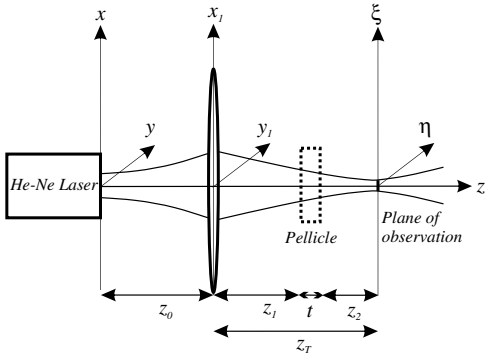

Fig. 1. Focusing of a Gaussian laser beam through a transparent pellicle in air by an ideal focusing lens. z_T is fixed and chosen to attain the best focusing conditions as described in the text. The dashed rectangle represents the sample.

There is a value of z_T in which the semi-width exhibits a minimum; for brevity this value will be referred as the best focusing distance and the corresponding transversal plane will be the best focusing plane.

As mentioned, for a full characterization of the propagation of the beam, we performed the overall propagation from the laser output up to the plane of observation. For simplicity in the description of our proposal this is not necessary; it is sufficient to begin our description by considering the beam distribution just after the lens. For this, let us consider a circular amplitude distribution of the Gaussian just at the back surface of the lens as [8],

$$\Psi(x_1, y_1) = A \exp\left(-\frac{x_1^2 + y_1^2}{r^2}\right) \exp[i\beta(x_1^2 + y_1^2)]. \tag{2}$$

In Eq. (2), A is a complex constant term, r is the semi-width of the Gaussian beam, and β is the corresponding coefficient of the convergent quadratic phase.

The field given by Eq. (2) is propagated up to the plane of observation. We obtain for the corresponding semi-width (r_A) at this plane [8]

$$r_A = \frac{r}{\pi}\sqrt{[\beta\lambda z_T + \pi]^2 + \frac{\lambda^2}{r^4} z_T^2}. \tag{3}$$

We emphasize that Eq. (3) corresponds to the case of the virtual pellicle.

By maintaining z_T constant, we now repeat the same calculation for a pellicle with geometrical thickness t and refractive index n. The semi-width r_B is now given as

$$r_B = \frac{r}{\pi}\sqrt{\left[\beta\lambda\left(z_1 + \frac{t}{n} + z_2\right) + \pi\right]^2 + \frac{\lambda^2}{r^4}\left(z_1 + \frac{t}{n} + z_2\right)^2}. \tag{4}$$

In writing Eq. (4), it has to be noticed that multiple reflections on the boundary do not affect the semi-width of the transmitted amplitude, as is typical when using pellicle beam splitters. On the contrary, the transmitted amplitude is drastically affected by multiple reflections.

It will be noticed from Eq. (4) that exactly the same value of r_B can be obtained with an uncountable set of samples that accomplishes

$$z_1 + \frac{t}{n} + z_2 = z_1' + \frac{t'}{n'} + z_2' = z_1'' + \frac{t''}{n''} + z_2'' = \cdots. \tag{5}$$

As z_T is fixed, combining Eq. (1) with Eq. (5) we obtain

$$t\frac{n-1}{n} = t'\frac{n'-1}{n'} = t''\frac{n''-1}{n''} = \cdots. \tag{6}$$

Equation (6) shows that the geometrical thickness multiplied by the ratio of the refractive index diminished in one over the refractive index is an invariant, provided z_T remains constant, which in our case corresponds to the best focusing plane. Moreover, the semi-width at the best focusing plane is independent of the position of the pellicle, that is, independent of the actual values of z_1 and z_2. This result demonstrates that piston-like movements (back and forth) of the pellicle under inspection do not affect the size of the Gaussian beam under measurement. Let us define an invariant factor F as

$$F = t\frac{n-1}{n}. \tag{7}$$

Equation (7) is the key in the calculations of the refractive index and geometrical thickness of our proposal described in Section 4.

From Eq. (4) it can be noticed that the value of t/n can be calculated by knowing r_B. However n and t cannot be calculated independently. To overcome this problem, we additionally use the equation of the power (P) transmitted by a pellicle in a homogeneous medium. This is a well-known equation [9,10] and for convenience is repeated here as

$$P = \left(\frac{4n_0n_1}{M}\right)^2, \tag{8}$$

where n_0 and n_1 are the refractive indices of the homogeneous medium and the pellicle, respectively, and

$$M = \begin{vmatrix} 1 & -1 & -1 & 0 \\ -n_0 & -n_1 & n_1 & 0 \\ 0 & \exp\left(-i\frac{2\pi}{\lambda}n_0n_1t\right) & \exp\left(i\frac{2\pi}{\lambda}n_0n_1t\right) & -1 \\ 0 & n_1\exp\left(-i\frac{2\pi}{\lambda}n_0n_1t\right) & -n_1\exp\left(-i\frac{2\pi}{\lambda}n_0n_1t\right) & -n_0 \end{vmatrix}. \tag{9}$$

Equations (8) and (9) are valid for plane waves and are applied here with reasonable accuracy, as the pellicle is preferable placed as close as possible to the focal plane, in the Rayleigh zone, where the wave is almost collimated.

Equations (8) and (9) will be combined with Eq. (4) to fulfill the information needed. For this, it is necessary to measure accurately the power of the Gaussian beam transmitted by the pellicle. Actually, what we require is the ratio of the power detected when the pellicle is present divided by the power detected without the pellicle. In turn, to measure the power by integrating the intensity of the Gaussian profile, it is necessary to measure with good accuracy the semi-widths of the beams under detection. This is done by means of a homodyne detector that is immune to spurious light, harmonics, and undesired DC components. In the following section, we describe our homodyne detector, and in Section 4 we describe its use in our proposal.

Before continuing with our description, we want to remark that it is not necessary to actually measure the geometrical distances depicted in Fig. 1 in the experimental setup. Instead of this, we use the homodyne detector described in the following section to characterize the overall experimental propagation of the Gaussian beam. Now, we use the theoretical setup of Fig. 1, which uses an ideal lens, and we fix the corresponding parameters properly to match both propagations. As both propagations coincide everywhere, both the theoretical and the experimental propagations are the same. As a consequence, when a thin sample is introduced in the focused beam, between the lens and the plane of detection, the theoretical model must also match with the experimental setup. In this way we have a model that allows us to determine the properties of the sample under study.

3. Homodyne Detector for Measuring the Semi-Width of a Focused Gaussian Beam

In this section we describe our homodyne detector to measure the semi-width of a focused Gaussian beam with high accuracy and repeatability. Figure 2 depicts the setup. A He–Ne laser beam ($\lambda = 632.8$ nm) is focused by means of lens (L) at the best focusing plane where a knife edge is placed. The lens has a working distance of 1 cm allowing the placement of the sample. An attenuator (A) is included to avoid damaging the optical components due to excessive heating. A photo diode whose sensitive area is much larger than the dimensions of the incoming beam is positioned behind the knife edge. The sample is placed between the focusing lens and the best focusing plane.

The knife edge is fixed to a flexure piezoelectric transducer (PZT) that vibrates the knife edge in a plane transversal to the optical axis at a frequency (f) of 10 Hz with small amplitude (δ_0) of approximately 0.5 μm. A flexure type PZT is preferred as it exhibits low tilt (less than 5 μrad) and high resolution of about 2 nm.

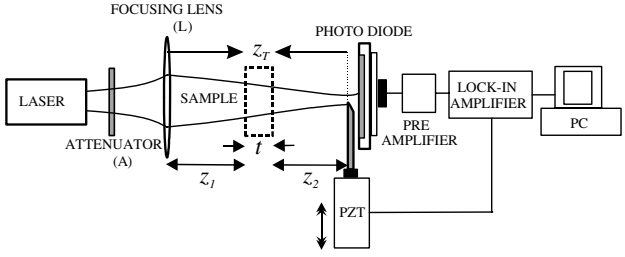

Fig. 2. Homodyne scanning system for determination of Gaussian semi-widths.

To describe how the vibrating knife edge allows us to determine the semi-width of the Gaussian beam in a homodyne way, we will consider the power collected by the photodiode of Fig. 2 as

$$P = A \int_{\alpha}^{\infty} \exp\left(-2\frac{x^2}{r_0^2}\right) dx. \tag{10}$$

Equation (10) represents the power collected by the photodiode as it integrates the overall beam excluding the portion covered by the knife edge. A is a constant scale factor, and the lower limit of the integral (α) represents the position of the knife edge.

Now, as the knife edge is vibrating, we can express the lower limit as

$$\alpha = x_0 + \delta_0 \cos(2\pi f t), \tag{11}$$

where x_0 is the static position of the vibrating knife edge. By substituting Eq. (11) in Eq. (10) and by performing an expansion in power series of the resulting equation, the linear term is of the form

$$P_{\text{linear}}(x_0) = B \exp\left(-2\frac{x_0^2}{r_0^2}\right) \cos(2\pi f t), \tag{12}$$

where B is a constant.

As the lock-in is tuned to the first harmonic, the signal results proportional to the intensity Gaussian profile evaluated at x_0, as indicated by Eq. (12). To obtain the overall profile, the knife edge is displaced in plane to different x_0 positions. In Fig. 3, plots of Gaussian distributions obtained experimentally are shown for the cases when the sample is present and without it.

In our experiments, the intensity spot size without the pellicle at the best focusing plane was approximately 2 μm. As the pellicle physically had to be placed away from this plane, we estimate that the pellicle was illuminated by a beam with a spot size of about 20 μm. Thus, our measurements represent a local value over this region. The corresponding power is obtained by integrating the area under the Gaussian distribution.

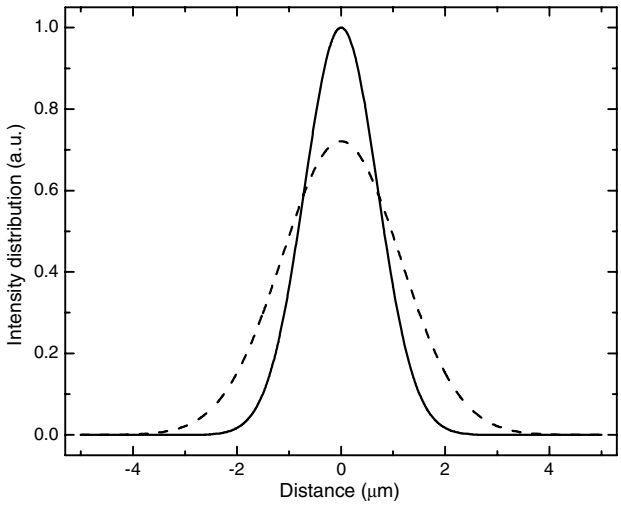

Fig. 3. Gaussian intensity distributions obtained experimentally without the sample (solid line) and with the sample included (dashed line).

(P_{air}), As all the parameters in the experiment are maintained fixed, B remains constant between measurements, allowing one to obtain the relative power (P_{rel}) as the ratio between the power when the sample is placed (P_{film}), referenced to the power measured without the sample (P_{air}),

$$P_{\text{rel}} = \frac{P_{\text{film}}}{P_{\text{air}}}. \tag{13}$$

Equation (13) represents a main parameter of our proposal. In the following section, we describe how to determine the geometrical thickness and refractive index of a sample consisting of a transparent pellicle in air.

4. Description of the Technique and Experimental Results

Once the semi-widths have been accurately measured with the homodyne detector, we proceed to assign to r_A and r_B in Eqs. (3) and (4) their corresponding values. The parameters r, β, and z_T were previously characterized and calculated numerically by means of the overall diffraction propagation of the beam.

Next we propose arbitrary values to z_1, z_2, and n to calculate its corresponding t value, taking care to fulfill with Eq. (1). In this manner, we have chosen one of the uncountable sets of possibilities that match with our experimental semi-width. With these values, we proceed in calculating the invariant factor F given by Eq. (7) and the relative transmitted power as given by Eq. (13).

At this point, it will be noticed that Eq. (8) contains sinusoidal terms on n and t. This behavior is illustrated in Fig. 4, which shows a plot of the transmitted power as a function of t calculated with the referred equation. In this plot, the corresponding relative power obtained experimentally is also included and represented with a solid horizontal line. The values of t in the plot are obtained by varying n in a range between 1.5 and 1.9 while maintaining fixed F given by Eq. (7). In Fig. 4 circles correspond to the intersection of the continuous possible powers with the experimentally obtained relative power.

It will be noticed that the plot in Fig. 4 is not periodic. This is a result of substituting Eq. (7) in Eq. (8), with n substituted by n_1.

As the only allowable values correspond to the intersection of both plots represented by circles in Fig. 4, now the set of possible geometrical thicknesses has been reduced to only 10 possibilities. It is now necessary to discern which one corresponds to the sample, and with the data available it is not possible. As a consequence, we have devised the following procedure.

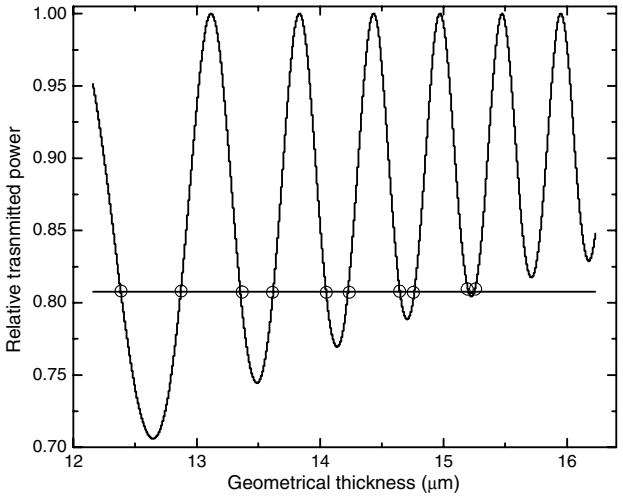

Fig. 4. Plot of the theoretical relative power transmitted by the sample as a function of its geometrical thickness obtained with Eq. (8) (oscillating plot). The horizontal line corresponds to the transmitted power measured experimentally. The circles represent the intersection of both plots (the allowable powers).

We displace the sample slightly to measure in a neighbor spot. At this new position, we measure again with the homodyne detector as it was done with the former measurement. For comparative purposes, we repeat Fig. 4 in Fig. 5, where plots of the second measurement represented by dashed lines have been added. In Fig. 5, circles represent the 10 possible values allowable for the first measurement, and squares represent the allowable 14 possible values for the second measurement.

At this point, we have calculated F for the first measurement and a corresponding F' for the second measurement. We have found a set of 10 possible thicknesses for the first measurement and 14 for

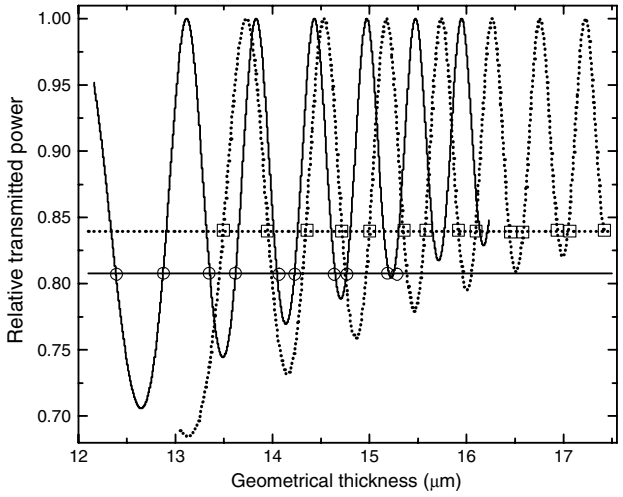

Fig. 5. Plots of the relative transmitted powers as a function of the geometrical thickness for two neighbor spots obtained with Eq. (8) in a similar way as Fig. 4. The horizontal lines correspond to the relative powers transmitted by the sample, which are measured experimentally as described in the text. Circles correspond to allowable values for the first measurement, squares for the second measurement.

Table 1. Values Obtained for the Refractive Index and Geometrical Thickness for Each Combination of the Three Measurements on the Stretch Film

Measurement	Spot1–Spot2	Spot2–Spot3	Spot1–Spot3
n_1	1.758	—	1.758
n_2	1.757	1.757	—
n_3	—	1.752	1.752
Δn	1×10^{-3}	5×10^{-3}	6×10^{-3}
t_1 (μm)	13.35	—	13.35
t_2 (μm)	14.34	14.34	—
t_3 (μm)	—	14.83	14.83

the second one. Now, with the refractive index being a characteristic of the material composition, it should remain basically constant on the small vicinity where the measurements were performed. Thus,

$$F = t\frac{n-1}{n}, \tag{14a}$$

$$F' = t'\frac{n-1}{n}, \tag{14b}$$

for each measurement, respectively, which allows us to divide Eq. (14a) by Eq. (14b) to eliminate n, as

$$\frac{F}{F'} = \frac{t}{t'}. \tag{15}$$

As F and F' are known values, Eq. (15) implies that the ratio of the thicknesses is also known. To determine t and t', we take all the combinations that correspond to the 10 values of the first measurement against the 14 values of the second one until the ratio fits better. In this way, all the non-allowable values are discarded, remaining only the pair t and t', which is the unique allowable solution. Finally, by using Eqs. (14a) and (14b), two refractive indices are obtained, n and n'. These two values are expected to be the same, but as they were obtained experimentally, an inherent small difference arises, and it is considered in the error uncertainty.

To verify the correctness of the results, we performed the same measurement on a third neighbor spot. Table 1 summarizes the results obtained.

Table 1 lists the experimental results obtained with our proposal of measuring with pairs of neighbor spots. The results confirm the correctness of our technique, as the results are consistent when measuring with different pairs. Obviously, more spots can be taken to improve the trustworthiness of the technique. For illustrative purposes, we have limited this report to only three. It is worth mentioning that the thickness reported by the manufacturer is in a range between 9 and 18 μm.

5. Conclusions

We have described and proved analytically and experimentally a technique based on the diffractive properties of Gaussian beams combined with the

equations of the transmitted light by a layer to measure locally the geometrical thickness and the refractive index of a transparent pellicle in air, supported only at its border. Under these conditions, the pellicle undergoes a continuous piston-like movement making interferometric techniques unfeasible to be used for this purpose. In contrast, we showed that our technique is immune against these movements, making it suitable for this application.

To remove ambiguities in the analytical equations due to oscillatory terms, we performed the measurements using combinations of neighbor pairs on the region under inspection of the sample; this allowed us to determine their corresponding local geometrical thicknesses and refractive index. This way of measuring can be taken as an advantage, as measuring with different combinations of neighbor pairs allowed us to confirm the consistency and correctness of each individual measurement.

References

1. www.filmetrics.com.
2. W. Vargas and D. Castro, "Closed equation for the normal incidence reflectance of thin films on absorbing substrates," Appl. Opt. **46**, 502–505 (2007).
3. C. Wang, J. Lin, H. Jian, and C. Lee, "Transparent thin-film characterization by using differential optical sectioning interference microscopy," Appl. Opt. **46**, 7460–7463 (2007).
4. P. Hlubina, D. Ciprian, J. Lunácek, and M. Lesnák, "Dispersive white-light spectral interferometry with absolute phase retrieval to measure thin film," Opt. Express **14**, 7678–7685 (2006).
5. M. Ramsteiner, C. Wild, and J. Wagner, "Interference effects in the Raman scattering intensity from thin films," Appl. Opt. **28**, 4017–4023 (1989).
6. Y. Cui and R. Azzam, "Determination of the refractive index and thickness of transparent pellicles by use of the polarization-independent absentee-layer condition," Appl. Opt. **35**, 5040–5043 (1996).
7. M. Cywiak, J. Murakowski, and G. Wade, "Beam blocking method for optical characterization of surfaces," Int. J. Imaging Syst. Technol. **11**, 164–169 (2000).
8. M. Cywiak, A. Morales, J. Flores, and M. Servín, "Fresnel-Gaussian shape invariant for optical ray tracing," Opt. Express **17**, 10564–10572 (2009).
9. E. Hecht, *Optics*, 2nd ed. (Addison-Wesley, 1987), pp. 426–431.
10. F. A. Jenkins and H. E. White, "Interference involving multiple reflections," in *Fundamentals of Optics*, 3rd ed. (McGraw-Hill, 1957), Chap. 14, pp. 260–264.

Refractive index and geometrical thickness measurement of thin optical samples by a transmitted Gaussian beam

Octavio Olvera-R,[1] Moisés Cywiak,[1,*] Joel Cervantes-L,[1] and David Cywiak[2]

[1]Centro de Investigaciones en Óptica A. C. León, Gto 37150, Mexico

[2]Centro Nacional de Metrología, Querétaro, Qro 76246, Mexico

*Corresponding author: moi@cio.mx

Received 11 August 2014; accepted 4 September 2014;
posted 11 September 2014 (Doc. ID 220750); published 14 October 2014

We describe a technique for simultaneously measuring the local geometrical thickness and the refractive index of semi-transparent thin plates by means of the diffractive properties of a transmitted Gaussian beam. The technique is based on measuring the semi-width of the transmitted beam and the shift of the Gaussian centroid caused by introducing a tilt on the sample under test. A homodyne technique is devised to accurately characterize the Gaussian beam. Our proposal does not require any prior information of the sample under study. We present analytical support of our technique and we give experimental results. © 2014 Optical Society of America

OCIS codes: (070.0070) Fourier optics and signal processing; (070.7345) Wave propagation; (120.0120) Instrumentation, measurement, and metrology; (120.3940) Metrology; (160.0160) Materials; (160.2750) Glass and other amorphous materials.

http://dx.doi.org/10.1364/AO.53.006993

1. Introduction

High-quality optical plates (OPs) have many applications; their performance depends on their refractive index and geometrical thickness and has to be measured with high accuracy, as is the case in flat panel displays, security window glasses, and windshields, among others. A variety of techniques for measuring these parameters have been reported, the interferometric techniques probably being the most used [1–12]. However, under an industrial environment, these methods are highly vulnerable to external noise even when used in holographic tables. Moreover, these methods are not able to provide the refractive index and geometrical thickness separately and must be combined with others, for example, low coherence interferometry combined with confocal microscopy [1–5], variants of wave-scanning interferometry [6–10], or a different focusing method based on a cyclic path optical configuration [11,12]. Most of these techniques are suitable for moderately thick samples (order of mm) and are difficult to implement for thinner plates (80–170 μm) because it becomes difficult to discern the focusing at both ends when the plate is very thin. As industry demands thinner plates, alternative techniques are required.

In this manuscript we describe a noninterferometric technique that allows for simultaneously measuring the refractive index and the local geometrical thickness of a thin OP. In principle, this technique can be applied to measure in a wider range. It can be considered an extension of our previous work reported in [13], where it is described how to measure the geometrical thickness and the refractive index of a transparent pellicle supported only by its border. In [13], the sample being a thin film, it was required using the analytical equations of a plane wave

1559-128X/14/306993-06$15.00/0

transmitted by a thin layer. In the technique reported here, the thin film equations cannot be applied due to the OP thickness (80–170 μm). Additionally, the sample does not need to be highly transparent as power measurements are not performed. In this proposal the refractive index and geometrical thickness are determined by measuring the semi-width of the transmitted Gaussian beam when it impinges normally to the sample and by determining the centroid position when the beam impinges obliquely by tilting the sample at different angles.

In the next sections, we describe our analytical proposal and give experimental results.

2. Analytical Description

We divide our description into two sections: characterization of the Gaussian beam through the system and shifting of the centroid beam due to tilting of the sample.

The characterization of the Gaussian beam is performed by means of the Fresnel diffraction integral. The centroid shift due to the sample tilt is calculated following geometrically the shift of the central ray of the Gaussian beam.

A. Propagation of the Gaussian Beam

The propagation of the Gaussian beam from the laser up to the detection plane is reported in [13]. It is repeated here for convenience.

In Fig. 1 the system is adjusted to focus the laser beam at the plane of observation with coordinates (ξ,η) in the absence of the sample, by means of a focusing lens placed on a coordinate plane (x_1,y_1) at a distance z_0 from the laser output. The lens is considered very thin, and the aperture is large enough to allow neglecting truncation of the beam. The plane of observation is adjusted at a distance z_T behind the lens to attain the best focusing conditions (minimum beam semi-width). We will refer to this plane as the best focusing plane. Once z_T has been fixed, the sample with geometrical thickness t is introduced transversely to the optical axis z in the optical path. It can be seen that

$$z_T = z_1 + t + z_2, \tag{1}$$

where z_1 and z_2 are the distances depicted in Fig. 1, which can be chosen arbitrarily, as will be demonstrated below.

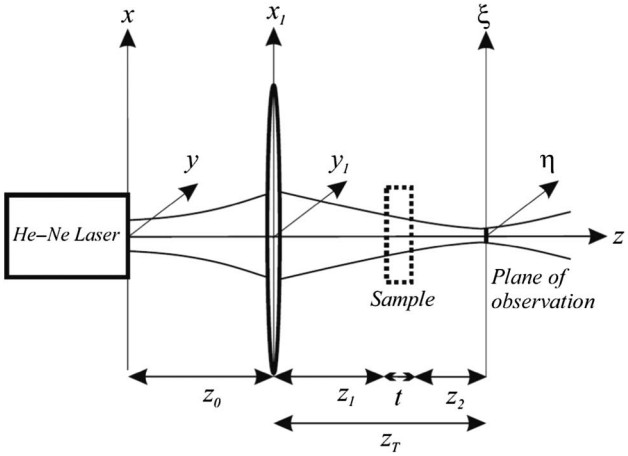

Fig. 1. Propagation of the Gaussian beam as described in the text. z_T is set such that the plane (ξ,η) corresponds to the best focusing plane.

For illustrative purposes the width of the sample has been exaggerated in Fig. 1.

The overall propagation of the Gaussian beam throughout the system can be calculated by means of the Fresnel diffraction integral [14].

We first consider a virtual sample, that is, a plate with a refractive index equal to 1 and geometrical thickness t. For this condition we calculate the overall propagation from the laser up to the plane of observation, and we plot the semi-width of the Gaussian beam as a function of distance z_T. These calculations allow characterizing of all the parameters involved in the propagation of the beam.

There is a value of z_T in which the semi-width exhibits a minimum at the plane of observation; this z_T value will be referred to as the best focusing distance, and the corresponding transversal plane is the best focusing plane.

As mentioned, for an overall characterization of the beam propagation, it is necessary to calculate the propagation from the laser output up to the plane of observation. For simplicity in the description of our proposal this is not necessary; it is sufficient to begin our description by considering the beam distribution just after the lens. For this, we consider a circular amplitude distribution of the Gaussian just at the back surface of the lens as [15]

$$\Psi_1(x_1,y_1) = A\,\exp\left(-\frac{x_1^2+y_1^2}{r^2}\right)\exp[-i\beta(x_1^2+y_1^2)]. \tag{2}$$

In Eq. (2) A is a complex constant term, r is the semi-width of the Gaussian beam, and β is the corresponding coefficient of the convergent quadratic phase.

The field given by Eq. (2) is propagated up to the plane of observation. We obtain for the corresponding semi-width (r_A) at this plane [15]

$$r_A = \frac{\sqrt{\lambda^2 z_T^2 + r^4(\beta\lambda z_T - \pi)^2}}{\pi r}. \tag{3}$$

We emphasize that Eq. (3) corresponds to the case of a virtual sample with a refractive index equal to 1. r_A, r, β, and λ are determined experimentally, as it will be described in Section 4. In this manner we propose a value for z_T that matches with our experimental conditions and it is unique.

By keeping z_T constant, we now repeat the same calculation for a plate with a refractive index n and geometrical thickness t. The semi-width r_B is given as

$$r_B = \frac{\sqrt{\lambda^2\left(z_T - t + \frac{t}{n}\right)^2 + r^4\left(\beta\lambda\left[z_T - t + \frac{t}{n}\right] - \pi\right)^2}}{\pi r}. \quad (4)$$

It will be noticed from Eq. (4) that exactly the same value of r_B can be obtained with an uncountable set of samples that accomplish

$$z_T - t + \frac{t}{n} = z_T - t' + \frac{t'}{n'} = z_T - t'' + \frac{t''}{n''} = \cdots, \quad (5)$$

where the primed values stand for the set of possible samples.

Considering that z_T is known and fixed, combining Eq. (1) with Eq. (5) we obtain

$$t\frac{n-1}{n} = t'\frac{n'-1}{n'} = t''\frac{n''-1}{n''} = \cdots. \quad (6)$$

Equation (6) shows that the geometrical thickness multiplied by the ratio of the refractive index diminished in one over the refractive index is an invariant, provided z_T remains constant, which does not necessarily have to correspond to the best focusing plane; we will see below that the measurements can be taken at any arbitrary plane. Moreover, the semi-width at the focusing plane is independent of the position of the sample, that is, independent of the actual values of z_1 and z_2, as can be seen from Eq. (4). Thus, back and forth movements of the plate under inspection do not affect the size of the Gaussian beam under measurement. An invariant factor F can be defined as

$$F = t\frac{n-1}{n}. \quad (7)$$

Equation (7) is one of the keys for calculating the refractive index and geometrical thickness in our proposal.

From Eq. (4) it can be noticed that the value of F can be calculated by measuring r_B. However, n and t cannot be calculated independently. To overcome this problem we introduce a tilt in the sample to cause a shift in the centroid of the Gaussian beam as described in the next section.

B. Shift of the Gaussian Centroid

In Fig. 2 a beam impinges on an OP of thickness t and refractive index n with an angle θ with respect to the normal N as depicted. We assume that the faces of the plate are parallels. As our technique measures in a very small spot of a high quality sample, this assumption seems reasonable.

The oblique incidence will cause two effects: first, the beam will travel a larger distance inside the sample, making the Gaussian beam wider at the plane of detection. It has to be remarked that this broadening of the beam is irrelevant for our proposal, as it is not necessary to measure the semi-width of the beam when the sample has been tilted; it is necessary to measure the semi-width only in the transversal case.

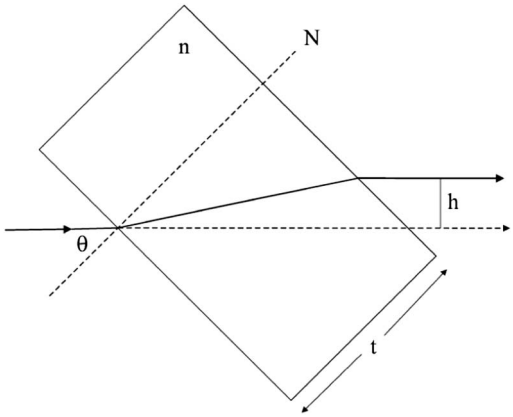

Fig. 2. Shifting (h) of the beam centroid due to a tilt (θ) of the sample.

The second effect caused by the tilting of the sample is a shift on the centroid at the plane of detection. The beam is shifted by an amount h given as

$$h = t\frac{\sin\theta\sqrt{n^2 - \sin^2\theta} - \sin\theta\cos\theta}{\sqrt{n^2 - \sin^2\theta}}. \quad (8)$$

Measuring the shift h and the beam semi-width at normal incidence allows using Eqs. (7) and (8) to calculate t and n.

Up to this point the bases of our proposal have been introduced. Before proceeding further it will be convenient to study the behavior of Eqs. (7) and (8) graphically. This is presented in the following section.

C. Theoretical Behavior of the Basic Equations

By combining Eqs. (7) and (8), we obtain

$$h = F\frac{n}{n-1}\frac{\sin\theta\sqrt{n^2 - \sin^2\theta} - \sin\theta\cos\theta}{\sqrt{n^2 - \sin^2\theta}}. \quad (9)$$

Experimentally measuring r_A, r_B, and z_T in Eqs. (3) and (4) allows us to determine values for n and t corresponding to the uncountable set of possible samples. Once n and t are fixed, F is known. Additionally if t is kept fixed, then it is possible to use Eq. (9) to plot h as a function of θ. Figure 3 depicts plots of h as a function of θ for an illustrative case of a sample with $t = 140$ μm and three different values of n: 1.4, 1.5, and 1.6.

From Fig. 3 it can be noticed that as the tilt increases the separation between the curves is also increasing. This indicates that higher accuracies can be obtained by measuring in a wide range of tilts, for example between 0° and 45°.

At this point it will be convenient to describe our homodyne detector used to perform the measurements of the semi-widths and centroids of the Gaussian beam with high accuracy.

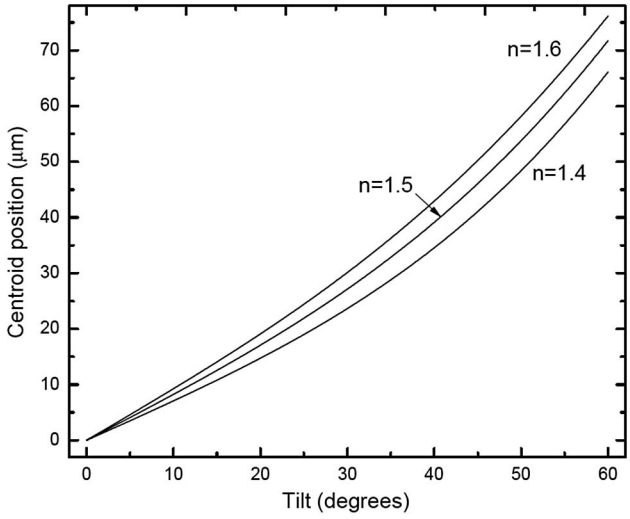

Fig. 3. Plots of the centroid position as a function of the tilt for three samples with $t = 140$ μm and $n = 1.4$, $n = 1.5$, and $n = 1.6$.

3. Homodyne Detector

As described in [13], the homodyne detector uses a vibrating knife edge as depicted in Fig. 4. The knife edge is placed at the detection plane. For our purposes, the lens has a working distance of 1 cm allowing the placement of the sample. The OP is mounted on a precision rotary stage (minimum step 0.5°). An attenuator (A) is included to avoid damaging the optical components due to excessive heating. A photodiode whose sensitive area is much larger than the spot size of the beam is positioned behind the knife edge. The knife edge is fixed to a flexure piezoelectric transducer (PZT) to vibrate in a plane transversal to the optical axis at a low frequency (f), in our case 10 Hz, with small amplitude (δ_0) of 500 nm. The PZT is also used to displace in plane the knife edge and has a high resolution of about 50 nm. A flexure type PZT is preferred, as it exhibits a low tilt of less than 5 μrad.

The vibrating knife edge allows for determining the semi-width of the Gaussian beam in a homodyne way as follows. First, when the knife edge is not vibrating, due to the photodiode large sensitive area, the power collected (P) can be written as

$$P = A \int_{\alpha}^{\infty} \exp\left(-2\frac{x^2}{r_0^2}\right) \mathrm{d}x. \tag{10}$$

In Eq. (10) A is a constant scale factor and the lower limit of the integral (α) represents the initial position of the knife edge. r_0 is the semi-width of the beam at the plane of detection. In summary, Eq. (10) establishes that the photodiode integrates the overall beam excluding the portion covered by the knife edge.

Now, when the knife edge is vibrating, the lower limit is written as

$$\alpha = x_0 + \delta_0 \cos(2\pi f t), \tag{11}$$

where x_0 is a static position. By substituting Eq. (11) in Eq. (10) and by performing an expansion in power series of the resulting equation, the linear term is

$$P_{\mathrm{linear}}(x_0) = B \exp\left(-2\frac{x_0^2}{r_0^2}\right) \cos(2\pi f t), \tag{12}$$

where B is a constant. Only the first order term of the expansion is considered because the lock-in amplifier is tuned to the first harmonic. Thus, the signal detected by the lock-in results proportional to the intensity Gaussian profile evaluated at x_0, as indicated by Eq. (12).

To obtain the overall shape of the Gaussian beam with our homodyne detector it is necessary to displace the position of the knife edge to different values of x_0. In this way, the profile and width of the Gaussian beam are obtained with high accuracy at the plane of detection.

In the next section we provide experimental results.

4. Experimental Section

With a commercially available translation stage we displace along the optical axis the homodyne detector, and we recorded the Gaussian profile at different positions. The minimum semi-width obtained corresponds to the best focusing conditions. At this plane, the values of z_T and r_A are registered. In our experiment r_A is approximately one micrometer. If the detector is maintained at this plane, the system will

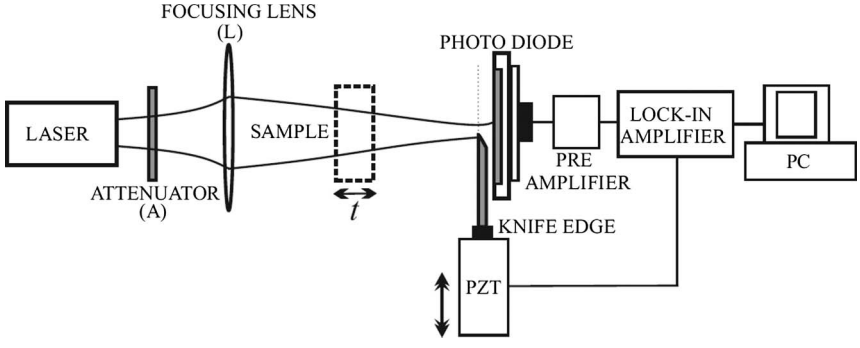

Fig. 4. Homodyne detector setup for measuring the semi-width and centroid of the transmitted Gaussian beam.

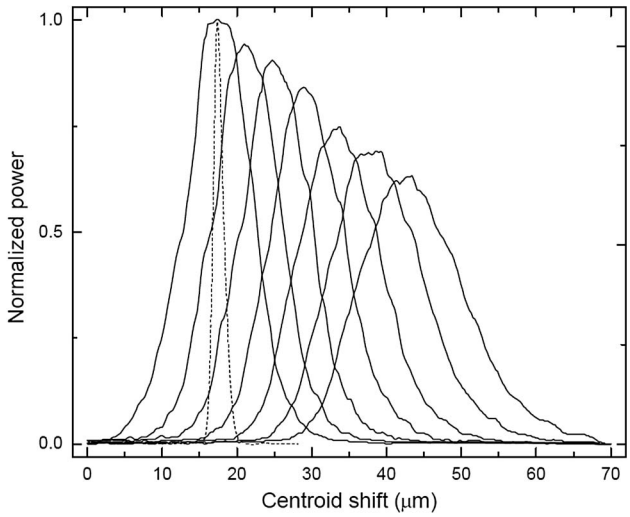

Fig. 5. Gaussian profiles measured with the homodyne detector from 0° to 30°. The narrowest profile (dashed line) is obtained without the sample, and its amplitude is reduced approximately six times. The solid lines are the profiles measured with the sample tilted at different angles. The solid line profile at the left corresponds to the zero tilt case. The 30° profile has the smaller vertical amplitude.

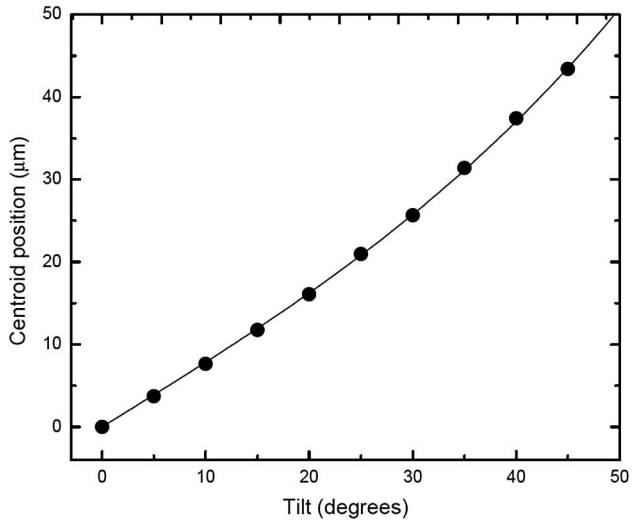

Fig. 6. Fitted theoretical curve adjusted to the experimental values (circles).

Table 1. Values for n and t by Using Our Proposed Technique Compared with the Values Reported by the Manufacturer

	n	t
Proposed technique	1.522 ($\lambda = 0.632$ μm)	129.6
Reported by manufacturer	1.523 ($\lambda = 0.589$ μm)	120–170

exhibit maximum sensitivity, which is desirable for very thin samples. If, as in our case, the expected geometrical thickness of the sample is in the range of 120–170 μm, it is convenient to displace the homodyne detector slightly from the best focusing plane because our PZT has a maximum scanning distance of 100 μm. For our experimental purposes this displacement is about 4.5 μm. The working conditions in our measurements were $\beta = 4.971 \times 10^8$ m^{-2}, $r = 2.2$ mm, $r_A = 1.4$ μm, $z_T = 1.0$ cm, $\lambda = 0.632$ μm.

Next, the sample is placed at normal incidence (zero tilt). Its placement is easily done as its corresponding centroid has to coincide with the one of the profile recorded without the sample. Under this condition r_B is determined. In our case, $r_B = 8.77$ μm with a corresponding value of $F = 44.45$ μm.

Finally the sample is tilted in steps of 5° up to 45° by means of a precision rotary stage, and the Gaussian profile is recorded for each case. Figure 5 shows plots of the profiles obtained. The plots are normalized with respect to the zero-tilt profile. For clarity, Fig. 5 exhibits profiles obtained up to 30°. The Gaussian profile measured without the sample is also included in the plot; its amplitude has been decreased about six times.

With the profiles recorded, a plot of the centroids as a function of the tilt is performed. Figure 6 depicts the experimental measurements (represented by circles) and the fitted theoretical curve obtained with Eq. (9). The fitting curve is determined with a least square method. The optimal value gives the expected sample value of n and its corresponding t. This method allows us to obtain n with a precision on the third decimal digit and t with a precision of a half micrometer, which in our case represents a precision of 0.4%.

Our sample consisted of a commercially available cover glass. The manufacturer sample characteristics compared with those obtained with our technique are given in Table 1.

The refractive index reported by the manufacturer is only available for $\lambda = 0.589$ μm.

Before finishing this report we want to remark that the sensitivity of the system may be increased by placing the homodyne detector in the best focusing plane in order to measure thinner samples. In contrast, for wider samples a defocus can be intentionally introduced or a larger range PZT can be used.

5. Conclusions

A technique capable of simultaneously measuring the refractive index and the geometrical thickness of semi-transparent thin OPs by means of the diffractive properties of a transmitted Gaussian beam has been proposed and proved. The technique is based on measuring the semi-width of the transmitted beam and the shift of the Gaussian centroid caused by a sample tilt. As the technique is not interferometric, it is shown to be robust and immune to external noise. To illustrate the feasibility of the technique we experimentally determined the refractive index and geometrical thickness of a commercially available cover glass.

References

1. S. Kim, J. Na, M. Kim, and B. Lee, "Simultaneous measurement of refractive index and thickness by combining low-coherence interferometry and confocal optics," Opt. Express **16**, 5516–5526 (2008).

2. M. Ohmi, H. Nishi, Y. Konishi, Y. Yamada, and M. Haruna, "High-speed simultaneous measurement of refractive index and thickness of transparent plates by low-coherence interferometry and confocal optics," Meas. Sci. Technol. **15**, 1531–1535 (2004).
3. H. Maruyama, S. Inoue, T. Mitsuyama, M. Ohmi, and M. Haruna, "Low-coherence interferometer system for the simultaneous measurement of refractive index and thickness," Appl. Opt. **41**, 1315–1322 (2002).
4. M. Haruna, M. Ohmi, T. Mitsuyama, H. Tajiri, H. Maruyama, and M. Hashimoto, "Simultaneous measurement of the phase and group indices and the thickness of transparent plates by low-coherence interferometry," Opt. Lett. **23**, 966–968 (1998).
5. T. Fukano and I. Yamaguchi, "Simultaneous measurement of thicknesses and refractive indices of multiple layers by a low-coherence confocal interference microscope," Opt. Lett. **21**, 1942–1944 (1996).
6. T. Fukano and I. Yamaguchi, "Separation of measurement of the refractive index and the geometrical thickness by use of a wavelength-scanning interferometer with a confocal microscope," Appl. Opt. **38**, 4065–4073 (1999).
7. F. Gao, H. Muhamedsalih, and X. Jiang, "Surface and thickness measurement of a transparent film using wavelength scanning interferometry," Opt. Express **20**, 21450–21456 (2012).
8. P. de Groot, "Measurement of transparent plates with wavelength-tuned phase-shifting interferometry," Appl. Opt. **39**, 2658–2663 (2000).
9. K. Hibino, B. Oreb, and P. Fairman, "Wavelength-scanning interferometry of a transparent parallel plate with refractive-index dispersion," Appl. Opt. **42**, 3888–3895 (2003).
10. G. Coppola, P. De Natale, S. De Nicola, P. Ferraro, M. Gioffre, and M. Iodice, "Thickness measurement of thin transparent plates with a broad-band wavelength scanning interferometer," IEEE Photon. Technol. Lett. **16**, 1349–1351 (2004).
11. Y. Kumar and S. Chatterjee, "Simultaneous determination of refractive index and thickness of moderately thick plane-parallel transparent glass plates using cyclic path optical configuration setup and a lateral shearing interferometer," Appl. Opt. **51**, 3533–3537 (2012).
12. Y. Kumar and S. Chatterjee, "Thickness measurement of transparent glass plates using a lateral shearing cyclic path optical configuration setup and polarization phase shifting interferometry," Appl. Opt. **49**, 6552–6557 (2010).
13. O. Olvera-R, M. Cywiak, J. Cervantes-L, and A. Morales, "Refractive index and geometrical thickness measurement of a transparent pellicle in air by Gaussian beam defocusing," Appl. Opt. **53**, 2267–2272 (2014).
14. M. Cywiak, J. Murakowski, and G. Wade, "Beam blocking method for optical characterization of surfaces," Int. J. Imaging Syst. Technol. **11**, 164–169 (2000).
15. M. Cywiak, A. Morales, J. Flores, and M. Servín, "Fresnel–Gaussian shape invariant for optical raytracing," Opt. Express **17**, 10564–10572 (2009).